A compliant ionic adhesive electrode with ultralow bioelectronic impedance

Liang Pan, Pingqiang Cai, Le Mei, Yuan Cheng, Yi Zeng, Ming Wang, Ting Wang, Ying Jiang, Baohua Ji, Dechang Li, and Xiaodong Chen**

Dr. L. Pan, Dr. P. Cai, Dr. Y. Zeng, Dr. M. Wang, Dr. T. Wang, Dr. Y. Jiang, Prof. X. Chen
Innovative Centre for Flexible Devices (iFLEX), Max Planck – NTU Joint Lab for Artificial Senses, School of Materials Science and Engineering, Nanyang Technological University, 50 Nanyang Avenue, 639798, Singapore
E-mail: chenxd@ntu.edu.sg

L. Mei
Biomechanics and Biomaterials Laboratory, Department of Applied Mechanics, Beijing Institute of Technology, Beijing 100081, China

Prof. B. Ji, Prof. D. Li
Institute of Applied Mechanics, Department of Engineering Mechanics, Zhejiang University, Hangzhou, 310027, China
E-mail: dcli@zju.edu.cn

Prof. B. Ji
Beijing Advanced Innovation Center for Biomedical Engineering, Beijing, 100191, China

Prof. Y. Cheng
Institute of High Performance Computing, A*STAR, 138632, Singapore

Keywords: compliant electrode, bioelectronic impedance, surface electromyography, low noise, prosthetic control

Abstract

Simultaneous implementation of high signals-noise ratio but low crosstalk is of great importance for the weak surface electromyography (sEMG) signals when precisely driving the prosthesis to perform the sophisticated activities. However, due to the gaps with the curved skin during muscle contraction, many electrodes have poor compliance with skin and suffer from high bioelectrical impedance. This causes serious noise and error in the recorded signals, especially the signals from the low-level muscle contraction. Here, we report a design of a compliant electrode based on adhesive hydrogel, alginate-polyacrylamide (Alg-PAAm), which eliminates those large gaps through the strong electrostatic interaction and abundant hydrogen bond with the skin. The obtained compliant electrode, behaving an ultralow bioelectrical

impedance to ~20 kΩ, can monitor even 2.1% maximal voluntary contraction (MVC) of muscle. Furthermore, benefiting from high SNR of >5:1 at low-level MVC, the crosstalk from irrelevant muscle was minimized through reducing the electrode size. Finally, as a proof of concept, a prosthesis is successfully demonstrated to inerrably grasp the needle based on the 9 mm^2 Alg-PAAm compliant electrode due to high SNR (~10:1) and no crosstalk. Our strategy to design such compliant electrodes provides the potential for improving the quality of dynamically weak sEMG signals to precisely control prosthesis in performing purposefully dexterous activity.

Ionic conduction in the biological system plays a central role in the transmission of vital signs and performing physiological activities, such as the transmission of nerve signals, muscle contraction, heart beating, blood pressure control, etc.[1-24] Highly efficiently and inerrably collecting or delivering these ionic signals are of great interest in clinical neurophysiology and material science for future wisdom medical and AI device controlling.[1, 25-30] Therefore, an electrode that complies with the curved biological surface and has low bioelectrical interfacial impedance (the ideal impedance of electrode-skin system is 6-10 kΩ which is the intrinsic impedance of skin) is on-demand to effectively couple the ionic fluxes in electrolytic tissues and electronic current in recording devices.[2, 3, 31] Surface electromyography (sEMG), involving the electrodes on skin, is a typical non-invasive and convenient technique to couple those two different currents.[32-35] Typically, two types of electrodes: dry and wet electrodes, distinguished by the ionic conducting layer between conductors and skin, can be applied for sEMG signals recording (Figure S1 and Table S1).[31, 36] However, many existing electrodes have micron-scale or larger gaps with the curved skin during muscle contraction (**Figure 1**a and Figure S1), which weaken the capacitive coupling process of ionic and electronic current. This poor compliance decreases the induced charge density at the bioelectronic interface and leads to high interfacial impedance with skin (ranges from high kΩ to low MΩ shown in Figure 1b).[15, 37-41] As a result, the high impedance produces high noise and distorts the recorded dynamic sEMG signals from muscle contraction, [40, 41] especially the contraction below 10% maximal voluntary contraction (MVC, a measure of the activity of muscles are relative to their maximum capabilities) from the sophisticated activities.[42] More importantly, the poor quality sEMG signal is harmful to restrain the crosstalk, the major problem in sEMG recording, through decreasing the size of the electrode.[43] Because sEMG measures the muscle activity from the surface of the skin as compared to needle and intramuscular EMG which focuses on single deep muscle.[44]

As described by Roger et al. previously,[37, 44] the total energy of interfacial contact ($U_{interface}$) consists of the bending energy of the electrode ($U_{bending}$) (mostly defined by the thickness of the electrode), the elastic energy of the skin (U_{skin}) and the adhesive energy of contact ($U_{adhesion}$), which is expressed as follows:

$$U_{interface} = U_{bending} + U_{skin} + U_{adhesion} \quad (1)$$

Accordingly, to minimize the interfacial gaps to comply with skin for low impedance, decreasing the thickness and improving the adhesion provide effective approaches for dry and wet electrodes, respectively (Figure 1b, Table S2 and Table S3).[37, 45-47] However, it remains a challenge to obtain lower bioelectronic impedance of dry electrode even when the thickness decreases to 100 nm.[16] For the wet electrode, achieving stronger adhesion between the conducting layer and skin is a key to eliminate the interfacial gaps. On the molecular level, this adhesion, avoiding any damage to the skin, is mainly attributed to the electrostatic and Van der Waals interaction between the ionic conducting layer of the electrode and stratum corneum (SC, the outermost layer of skin).[40, 48, 49] The SC has been likened to a brick wall structure, in which the corneocytes (i.e., the bricks) are embedded in the continuous matrix of specialized lipids (i.e., the mortar).[50, 51] The lipids form the outermost interface of SC, mainly composed of a heterogeneous mixture of long-chain ceramid (CER), cholesterol (CHOL), and free fatty acid (FFA) in certain ratios.[50-53] Introducing a compliant layer, which could form strong intermolecular interaction with CER, CHOL and FFA, to enhance the adhesion and form a non-gapped interface is a possible approach for high-quality sEMG signals from dynamically weak and fine muscle activities.

Here, we report the design of a compliant electrode which successfully eliminates the micro-scaled gaps with the skin due to the strong electrostatic and Van der Waals interaction. As a result, it has an ultralow impedance of ~20 KΩ with skin, which is lower than the current electrodes including commercial electrodes (~500 KΩ) (green star in Figure 1b). This compliant electrode is constructed by an adhesive ionic conducting hydrogel, alginate-

polyacrylamide (Alg-PAAm) containing 5 wt% of LiCl, which can generate strong electrostatic interaction and abundant hydrogen bond with SC of skin. Therefore, the adhesive force (90 N/m) of our electrode with skin is two times of commercial electrodes (41 N/m). Unlike commercial electrodes that can monitor muscle contractions only down to 7.2% MVC, our Alg-PAAm compliant electrode detects contractions down to 2.1% MVC. Moreover, even at low-level muscle contraction (<10% MVC, because most of muscle contraction from the sophisticated activities are below 10% MVC), our compliant electrode still has high SNR of >5:1, which is available for prosthetic control.[29] Due to the high SNR, the crosstalk from irrelevant muscles is minimized through reducing the size of Alg-PAAm electrode. Finally, as a proof of concept, we successfully drive a prosthetic hand to grasp a needle without errors based on the 9 mm^2 Alg-PAAm compliant electrode. Our strategy for such compliant electrodes provides the potential for minimizing the large gaps to improve the precision of dynamically weak sEMG signals and thus control prosthesis with purposeful activity.

Alg-PAAm is a typical highly adhesive hydrogel fabricated by Z. Suo et al. whose chains are built up by poly-alginate and polyacrylamide chains, cross-linked by covalent bonds (**Figure 2**a and Figure S2).[43, 49, 54] It has the highest adhesive (~1000 J/m^2) energy on wet and dynamic surfaces due to the high intermolecular interaction, which benefits the elimination of the micron-scale or lager gaps between the electrodes and skin. Figure 2b, Figure 2c, Figure S3 and Movie S1 show the process of molecular interaction between Alg-PAAm molecule and SC matrix. With the increasing of electrostatic and Van der Waals interaction, the distance between Alg-PAAm hydrogel molecule and SC gradually decreased (Figure 2d and Figure 2e). In addition, the number of H-bonds and atom contacts between the Alg-PAAm gel and SC matrix also increased (Figure 2f and Figure S4). Thus, the Alg-PAAm electrode was expected to have strong adhesion with the skin for minimizing large gaps. Here we employ the commercial electrode as a comparison because it has broad applications in prosthetic control. Firstly, we measured the adhesive force of Alg-PAAm through a 90° peel-off test on pigskin

(pigskin has a similar structure with human skin) and a 180° peel-off test, then compared that with commercial electrodes. In the 90° peel-off test, the Alg-PAAm compliant electrode showed an adhesive force of 90 N/m that is twice that of commercial electrodes (41 N/m) (Figure 2g and Figure S5). Similarly, in the 180° peel-off test, the compliant electrode remained superior to commercial electrodes (Figure S6). More importantly, cross-section SEM images show that the Alg-PAAm electrode has no gaps with the pigskin (Figure 2h) whereas many micron-scale gaps were seen for the commercial ones (Figure 2i). This is expected to improve the compliance with skin and decrease the impedance of the bioelectronic interface to optimize the coupling process between ionic fluxes in the skin and electronic current in the compliant electrode.

To improve the ionic conductivity of Alg-PAAm, we introduced 5 wt% LiCl into the hydrogel network. The resulting hydrogel had an intrinsic impedance of 270 Ω (the impedance of the hydrogel without LiCl is ~MΩ at 1 Hz), which is similar to commercial electrodes of 210 Ω at 1 Hz. Because of its flexibility and stretchability, the impedance of our electrode (the fabricated process shown in Figure S7) was nearly unchanged under 0-50% strains that are relevant to human movements when sEMG recordings were applied (Figure S8). As shown in Figure 2j, the impedance of the Alg-PAAm electrode-skin system is about 20 kΩ at 1 Hz, while the impedance of the commercial electrode-skin system is ~500 kΩ at 1 Hz. Also, this value is lower than other electrodes reported in previous works (Figure 1b). The ideal impedance of electrode-skin is 6-10 kΩ which is the intrinsic impedance of skin (the target impedance in Figure 1b).

To determine whether an electrode can detect weak sEMG signals that arise from fine but weak muscle activities, it is important to identify the recording limit of the electrode. Due to the low intensity of the coupling process between ionic and electron current, electrodes with high interfacial impedance caused by gaps at the electrode-skin interface cannot record these intrinsically weak signals. We obtained serial dynamic sEMG signals of muscle contractions

ranging from 1.5% MVC to 22% MVC using 9 mm^2 and 81 mm^2 Alg-PAAm compliant electrodes and 9.8 mm^2 and 78.5 mm^2 commercial electrodes (**Figure 3**a). The recording limit for both sizes of Alg-PAAm electrodes was 2.1% MVC while the limit for the 78.5 mm^2 commercial electrode was poorer at 7.2% MVC. No signals were recorded from the 9.8 mm^2 commercial electrodes when muscles contracted below 22% MVC. These results show that Alg-PAAm electrodes are more sensitive than commercial electrodes. Then, we compared the SNR of sEMG signals obtained at different muscle contractions using the four different sized electrodes. The highly adhesive Alg-PAAm electrode showed larger SNR (>5:1 which is useful for prosthetic controlling) than commercial electrodes (Figure 3b).[29] Also, at 20% MVC, regardless of electrode type, SNR increased with increasing electrode area (Figure S9). Alg-PAAm electrodes ≥9 mm^2 showed better SNR than the 78.5 mm^2 commercial electrodes.

Then, we used the high-quality sEMG signals recorded by Alg-PAAm compliant electrodes to drive a 3D-printed prosthetic finger to perform a low strength movement along with a human finger. Here, sEMG signals of 5% MVC were used as input to move the prosthesis. As shown in Figure S10 and Movie S2, using the compliant electrodes, the prosthetic thumb moved and bent according to the human thumb. Because of the high interfacial impedance of commercial electrodes, no sEMG signals were recorded and therefore, the prosthesis could not be driven to perform any activities alongside the human hand (Figure S11 and Movie S3).

One of the biggest problems in surface EMG is crosstalk-noise that arises from the interaction between two or more muscle units.[55] Because sEMG measures the muscle activity from the surface of the skin as compared to needle and intramuscular EMG which focuses on single deep muscle.[44] The crosstalk will contaminate signals and causes misinterpretation and is particularly problematic for dynamical weak signals that are used to control fine and precise movements. Therefore, minimizing the crosstalk to improve the precision of the sEMG signal is important for prosthetic control. Currently, the effective solution is decreasing the size of the

electrode as shown in Figure S12a.[56] Unfortunately, that will make the recorded sEMG signals poor, especially the weak signals from low-level muscle contraction. But for our compliant electrode, from Figure 3b, the SNR at 9 mm^2 under 5% MVC is larger than 5:1 which is enough for controlling the prostheses.[29] Thus, the Alg-PAAm compliant electrode is suitable for overcoming the possible crosstalk.

To assess the crosstalk rate, we placed the electrodes at the relevant positions according to the muscle distribution of the thumb (abductor pollicis longus), index (flexor carpi ulnaris), middle (flexor digitorum superficialis) and ring (palmaris longus) fingers (Figure S12b). Due to the relevant independence between abductor pollicis longus and the other three muscles, we measured the intensity of sEMG signals recorded from all fingers as the thumb moved. Then, we can assess the SNR of the signals from the thumb moving and the crosstalk rate of the signals from the other three fingers induced by thumb moving. Figure 3c shows the SNR and crosstalk rate (from the middle finger when thumb moving) based on our compliant and the commercial electrode at 10% MVC with the size from ~80 mm^2 to 1 mm^2. Generally, for both electrodes, SNR was decreased and the crosstalk rate was gradually minimized when the size of the electrode reduced. But the difference is that the SNR of the Alg-PAAm electrode was over 5:1, which is better than the commercial electrode. Benefitting from the high SNR, the crosstalk was successfully overcome when the size is below 9 mm^2. Nevertheless, the commercial electrode nearly cannot record the sEMG signals at 10% MVC when the size of the electrode is below 9 mm^2. Because of poor SNR of the smaller commercial electrode (Figure 3c), we used the Alg-PAAm compliant electrode to study the influence of crosstalk from adjacent muscles when we drove the protheses.

Figure 3d and Figure S13 show the crosstalk rate of the middle finger induced by the thumb with different electrode size and intensity of muscle contraction. When the size of the Alg-PAAm electrode was < 4 mm^2, no sEMG signals from the thumb were recorded, and accordingly, no crosstalk rates were measured when the muscular strength ranged from 5 to

100% MVC (means signal loss indicated by the dull red region in Figure 3d). For Alg-PAAm electrodes ≥9 mm^2, the crosstalk rate gradually increased with increasing electrode size and strength of muscle activity. Interestingly, there was a region of no crosstalk for electrode sizes between 4 and 25 mm^2 and muscle contraction intensity between 5 and 10% MVC. Like the crosstalk of middle finger induced by the thumb, the crosstalk rate of other fingers also depends on the size of the electrode and intensity of muscle contraction, i.e., less crosstalk is observed with smaller electrodes and lower intensity muscle contractions. Figure 3e shows the sEMG signals of all fingers (recorded by 9 mm^2 Alg-PAAm electrode at 10% MVC) from the crosstalk-free region shown in Figure 3d. No crosstalk signals were detected in the other fingers when the thumb moved. Figures S14-16 show a detailed comparison of the sEMG signals from the different fingers at 100%, 60%, 20%, and 10% MVC obtained using different size commercial and compliant electrodes. Both the large Alg-PAAm (81 mm^2) and commercial electrode (78.5 mm^2) had higher levels of crosstalk than small Alg-PAAm electrodes (9 mm^2) (Figure S17). Due to poor SNR (Figure 3c) induced by gaps shown in Figure 2h, commercial electrodes below 20 mm^2 cannot record any signals. In the case of our compliant electrodes that were ≤9 mm^2 and highly adhesive, the crosstalk from adjacent muscles disappeared when the muscle contraction was below 10% MVC, making them suitable for monitoring low-level muscle contractions from human fingers.

Using sEMG signals to drive prostheses to perform fine and sophisticated activities such as grasping needles has long been desired.[1, 25, 26] As a proof-of-concept, we used our Alg-PAAm compliant electrodes to record sEMG signals from the fingers of a normal human hand and use these signals to drive a 3D-printed prosthetic hand to grasp a needle. The large 78.5 mm^2 commercial electrodes were used as a comparison. We firstly recorded sEMG signals of the thumb, index, middle, and ring fingers when the human hand grasped the needle. These signals were then used as the programmed input to drive the prosthesis to mirror the grasping of a needle. Here, we define the intensity of signals as important factors correlated with the

bending angle of the fingers (Max intensity = Max bending angle). **Figures** 4a-4c and Movie S4-S6 show the grasping process based on 78.5 mm^2 commercial electrode and 81 mm^2 and 9mm^2 Alg-PAAm electrodes (because of the commercial electrode < 20 mm^2 cannot record any signals at low-level MVC, here we did not used 9.8 mm^2 commercial electrodes as a comparison). Green arrows in the figures are dynamic bio-signals generated by the thumb and index finger when grasping the needle. As seen in Figure 4d, the recorded sEMG signals showed crosstalk from the middle and ring fingers (marked with blue ovals in Figure 4a). Based on the intensity of the recorded sEMG, an electrical signal (red arrows in Figure 4a) is subsequently applied to control the movement of the prosthetic finger. Figure 4e shows the bending angle of all fingers driven by the sEMG signals. Although the prosthetic thumb and index finger moved according to the motion of the human finger, the prosthesis still failed to catch the needle due to signal distortion induced by high impedance of the commercial electrode-skin system. Furthermore, crosstalk had caused the prosthetic middle and ring fingers to move even though no movements were made in the respective human fingers.

In the case of the Alg-PAAm electrodes (Figure 4b and Figure 4c), the prosthetic thumb and index fingers successfully grasped the needle alongside the human hand (Movies S5, S6). However, when using sEMG signals from 81 mm^2 Alg-PAAm electrodes as input, the middle and ring fingers also bent by an undesirable 5-10° due to the crosstalk (Figures 4f and 4g). With the 9 mm^2 Alg-PAAm electrodes, the crosstalk from the ring finger was minimized to the range of background noise and therefore, the finger remained stationary (Figure 4h and 4i). Here the slight movement with 1-2° of the middle finger in Figure 4i was induced from the friction between middle and index finger which is the design bug of 3D-printed materials (not from the crosstalk). These results show that the electrode-skin interface without micron-gaps and small electrode size are crucial for the precision of the sEMG signals when driving prosthetic devices to perform fine and sophisticated activities like humans.

In conclusion, we successfully design the compliant ionic adhesive electrode that can record dynamically weak sEMG signals with low crosstalk for driving a prosthetic finger to perform fine activities such as grasping a needle. We employed the highly adhesive Alg-PAAm hydrogel containing 5% LiCl as a compliant layer to enhance the intermolecular interaction to eliminating the micron-gaps on the skin. Our Alg-PAAm compliant electrode has a lower bioelectrical impedance (20 kΩ) with skin and better SNR than commercial electrodes (~500 kΩ) at low-level muscle contraction. As a result, our electrode can record weak sEMG signals even at muscle activities of 2.1% MVC. More importantly, the smaller Alg-PAAm electrodes were better at minimizing undesirable crosstalk from adjacent muscles. And, the weak sEMG signals recorded by our compliant electrode from a human hand was used to drive the fingers of a prosthetic hand to grasp a needle without errors. Maneuvering current prostheses is difficult and tiring because they cannot yet perform sophisticated functions and typically use large power (>10% MVC) for small movements. Our results offer a promising solution for prosthesis users to perform fine and sophisticated movements using dynamically weak sEMG signals.

Supporting Information
Supporting Information is available from the Wiley Online Library or from the author.

Acknowledgements
This work was supported by the Agency for Science, Technology and Research (A*STAR) under its AME Programmatic Funding Scheme of Cyber-Physiochemical Interfaces Programme (project no. A18A1b0045), the National Research Foundation (NRF), Prime Minister's Office, Singapore, under its NRF Investigatorship (NRF-NRFI2017-07), Singapore Ministry of Education (MOE2019-T2-2-022), National Natural Science Foundation of China (NSFC 11932017, 11772054, 11772055, and 11532009), and the Fundamental Research Funds for the Central Universities (Grant No. 2019QNA4060). We also gratefully acknowledge the use of computing resources at the A*STAR Computational Resource Centre and National Supercomputing Centre, Singapore.

Received: ((will be filled in by the editorial staff))
Revised: ((will be filled in by the editorial staff))
Published online: ((will be filled in by the editorial staff))

References

[1] G. Buzsáki, C. A. Anastassiou, C. Koch, *Nat. Rev. Neurosci.* **2012**, *13*, 407.

[2] C. Yang, Z. Suo, *Nat. Rev. Mater.* **2018**, *3*, 125.

[3] H. Yuk, B. Lu, X. Zhao, *Chem. Soc. Rev.* **2019**, *48*, 1642.

[4] T. Wang, M. Wang, L. Yang, Z. Li, X. J. Loh, X. Chen, *Adv. Mater.* **2020**, *32*, 1905522.

[5] C. Wan, K. Xiao, A. Angelin, M. Antonietti, X. Chen, *Adv. Intell. Syst.* **2019**, *1*, 1900073.

[6] M. W. Schwartz, S. C. Woods, D. Porte, R. J. Seeley, D. G. Baskin, *Nature* **2000**, *404*, 661.

[7] D. Borton, S. Micera, J. d. R. Millán, G. Courtine, *Sci. Transl. Med.* **2013**, *5*, 210rv2.

[8] Y. Khan, A. E. Ostfeld, C. M. Lochner, A. Pierre, A. C. Arias, *Adv. Mater.* **2016**, *28*, 4373.

[9] W. Gao, S. Emaminejad, H. Y. Y. Nyein, S. Challa, K. Chen, A. Peck, H. M. Fahad, H. Ota, H. Shiraki, D. Kiriya, *Nature* **2016**, *529*, 509.

[10] Y. H. Jung, B. Park, J. U. Kim, T. i. Kim, *Adv. Mater.* **2019**, *31*, 1803637.

[11] G. Chen, N. Matsuhisa, Z. Liu, D. Qi, P. Cai, Y. Jiang, C. Wan, Y. Cui, W. R. Leow, Z. Liu, S. Gong, K. Zhang, Y. Chen, X. Chen, *Adv. Mater.* **2018**, *30*, 1800129.

[12] K. He, Y. Liu, M. Wang, G. Chen, Y. Jiang, J. Yu, C. Wan, D. Qi, M. Xiao, W. R. Leow, H. Wang, M. Antonietti, X. Chen, *Adv. Mater.* **2020**, *32*, 1905399.

[13] D. Qi, Z. Liu, Y. Liu, Y. Jiang, W. R. Leow, M. Pal, S. Pan, H. Yang, Y. Wang, X. Zhang, J. Yu, B. Li, Z. Yu, W. Wang, X. Chen, *Adv. Mater.* **2017**, *29*, 1702800.

[14] X. Yan, Z. Liu, Q. Zhang, J. Lopez, H. Wang, H.-C. Wu, S. Niu, H. Yan, S. Wang, T. Lei, J. Li, D. Qi, P. Huang, J. Huang, Y. Zhang, Y. Wang, G. Li, J. Tok, X. Chen, Z. Bao, *J. Am. Chem. Soc.* **2018**, *140*, 5280.

[15] M. K. Choi, O. K. Park, C. Choi, S. Qiao, R. Ghaffari, J. Kim, D. J. Lee, M. Kim, W. Hyun, S. J. Kim, *Adv. Healthc. Mater.* **2016**, *5*, 80.

[16] A. Miyamoto, S. Lee, N. F. Cooray, S. Lee, M. Mori, N. Matsuhisa, H. Jin, L. Yoda, T.

Yokota, A. Itoh, *Nat. Nanotechnol.* **2017**, *12*, 907.

[17] H. Yang, S. Ji, I. Chaturvedi, H. Xia, T. Wang, G. Chen, L. Pan, C. Wan, D. Qi, Y.-S. Ong, X. Chen, *ACS Mater. Lett.* **2020**, *2*, 478.

[18] S. Ji, C. Wan, T. Wang, Q. Li, G. Chen, J. Wang, Z. Liu, H. Yang, X. Liu, X. Chen, *Adv. Mater.* 2020, DOI:10.1002/adma.202001496.

[19] Z. Liu, X. Wang, D. Qi, C. Xu, J. Yu, Y. Liu, Y. Jiang, B. Liedberg, X. Chen, *Adv. Mater.* **2017**, *29*, 1603382.

[20] L. Pan, F. Wang, Y. Cheng, W. R. Leow, Y.-W. Zhang, M. Wang, P. Cai, B. Ji, D. Li, X. Chen, *Nat. Commun.* **2020**, *11*, 1332.

[21] S. Choi, H. Lee, R. Ghaffari, T. Hyeon, D. H. Kim, *Adv. Mater.* **2016**, *28*, 4203.

[22] P. Cai, C. Wan, L. Pan, N. Matsuhisa, K. He, Z. Cui, W. Zhang, C, Li, J. Wang, J. Yu, M. Wang, Y. Jiang, G. Chen, X. Chen., *Nat. Commun.* **2020**, *11*, 2183.

[23] S. R. Krishnan, T. R. Ray, A. B. Ayer, Y. Ma, P. Gutruf, K. Lee, J. Y. Lee, C. Wei, X. Feng, B. Ng, *Sci. Transl. Med.* **2018**, *10*. eaat8437.

[24] Y. Khan, A. E. Ostfeld, C. M. Lochner, A. Pierre, A. C. Arias, *Adv. Mater.* **2016**, *28*, 4373.

[25] K. A. Wheeler, D. K. Kumar, H. Shimada, *J Med Biol Eng* **2010**, *30*, 393.

[26] D. Hofmann, N. Jiang, I. Vujaklija, D. Farina, *IEEE Trans. Neural Syst. Rehabil. Eng.* **2015**, *24*, 1333.

[27] M. Zecca, S. Micera, M. C. Carrozza, P. Dario, *Crit. Rev. Biomed. Eng.* **2002**, *30*, 459.

[28] L. R. Hochberg, D. Bacher, B. Jarosiewicz, N. Y. Masse, J. D. Simeral, J. Vogel, S. Haddadin, J. Liu, S. S. Cash, P. Van Der Smagt, *Nature* **2012**, *485*, 372.

[29] S. Raspopovic, M. Capogrosso, F. M. Petrini, M. Bonizzato, J. Rigosa, G. Di Pino, J. Carpaneto, M. Controzzi, T. Boretius, E. Fernandez, *Sci. Transl. Med.* **2014**, *6*, 222ra19.

[30] N. G. Jablonski, *Annu. Rev. Anthropol.* **2004**, *33*, 585.

[31] S. F. Cogan, *Annu. Rev. Biomed. Eng.* **2008**, *10*, 275.

[32] H. J. Hermens, B. Freriks, R. Merletti, D. Stegeman, J. Blok, G. Rau, C. Disselhorst-Klug, G. Hägg, *Roessingh research and development* **1999**, *8*, 13.

[33] E. Criswell, *Cram's introduction to surface electromyography*, Jones & Bartlett Publishers, 2010.

[34] D. Winter, A. J. Fuglevand, S. Archer, *J. Electromyogr. Kinesiol.* **1994**, *4*, 15.

[35] F. V. Tenore, A. Ramos, A. Fahmy, S. Acharya, R. Etienne-Cummings, N. V. Thakor, *IEEE Trans. Biomed. Eng.* **2008**, *56*, 1427.

[36] M. A. Yokus, J. S. Jur, *IEEE Trans. Biomed. Eng.* **2015**, *63*, 423.

[37] J. W. Jeong, W. H. Yeo, A. Akhtar, J. J. Norton, Y. J. Kwack, S. Li, S. Y. Jung, Y. Su, W. Lee, J. Xia, H. Cheng, Y. Huang, W. Choi, T. Bretl, J. A. Rogers, *Adv. Mater.* **2013**, *25*, 6839.

[38] C. Pang, J. H. Koo, A. Nguyen, J. M. Caves, M. G. Kim, A. Chortos, K. Kim, P. J. Wang, J. B. H. Tok, Z. Bao, *Adv. Mater.* **2015**, *27*, 634.

[39] T. Yamamoto, Y. Yamamoto, *Med. Biol. Eng. Comput* **1977**, *15*, 219.

[40] M. M. Puurtinen, S. M. Komulainen, P. K. Kauppinen, J. A. Malmivuo, J. A. Hyttinen, "Measurement of noise and impedance of dry and wet textile electrodes, and textile electrodes with hydrogel", presented at *2006 International Conference of the IEEE Engineering in Medicine and Biology Society*, 2006.

[41] C. Pylatiuk, M. Muller-Riederer, A. Kargov, S. Schulz, O. Schill, M. Reischl, G. Bretthauer, "Comparison of surface EMG monitoring electrodes for long-term use in rehabilitation device control", presented at *2009 IEEE International Conference on Rehabilitation Robotics*, 2009.

[42] J. Woods, B. Bigland-Ritchie, *Am. J. Phys. Med.* **1983**, *62*, 287.

[43] C. J. De Luca, *J. Appl. Biomech.* **1997**, *13*, 135.

[44] S. Wang, M. Li, J. Wu, D.-H. Kim, N. Lu, Y. Su, Z. Kang, Y. Huang, J. A. Rogers, *J. Appl. Mech.* **2012**, *79*. 031022

[45] K. I. Jang, H. N. Jung, J. W. Lee, S. Xu, Y. H. Liu, Y. Ma, J. W. Jeong, Y. M. Song, J. Kim, B. H. Kim, *Adv. Funct. Mater.* **2016**, *26*, 7281.

[46] L. Bareket, L. Inzelberg, D. Rand, M. David-Pur, D. Rabinovich, B. Brandes, Y. Hanein, *Sci. Rep.* **2016**, *6*, 25727.

[47] J.-H. Kim, S.-R. Kim, H.-J. Kil, Y.-C. Kim, J.-W. Park, *Nano Lett.* **2018**, *18*, 4531.

[48] S. Kabiri Ameri, R. Ho, H. Jang, L. Tao, Y. Wang, L. Wang, D. M. Schnyer, D. Akinwande, N. Lu, *ACS nano* **2017**, *11*, 7634.

[49] K. S. Wu, W. W. van Osdol, R. H. Dauskardt, *Biomaterials* **2006**, *27*, 785.

[50] C. R. Harding, *Dermatol. Ther.* **2004**, *17*, 6.

[51] R. Notman, J. Anwar, *Adv. Drug Deliv. Rev.* **2013**, *65*, 237.

[52] R. Gupta, B. Rai, *J. Phys. Chem. B* **2015**, *119*, 11643.

[53] R. Gupta, D. Sridhar, B. Rai, *J. Phys. Chem. B* **2016**, *120*, 8987.

[54] J.-Y. Sun, X. Zhao, W. R. Illeperuma, O. Chaudhuri, K. H. Oh, D. J. Mooney, J. J. Vlassak, Z. Suo, *Nature* **2012**, *489*, 133.

[55] D. Farina, R. Merletti, B. Indino, M. Nazzaro, M. Pozzo, *Muscle Nerve* **2002**, *26*, 681.

[56] S. Day, *Bortec Biomedical Ltd publishers:Calgary, AB, Canada*, **2002**, pp. 1-17.

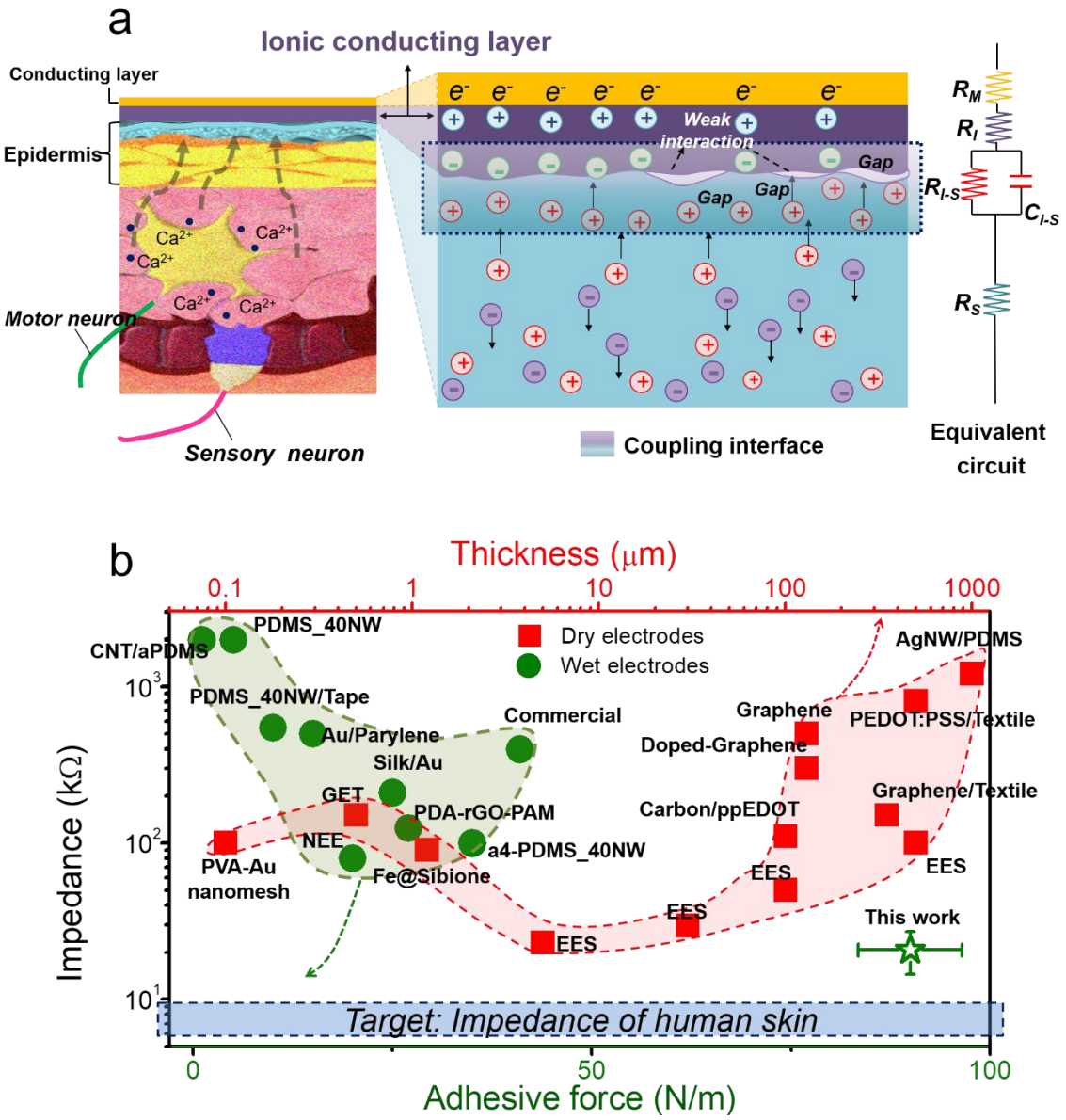

Figure 1. Ultralow bioelectrical interfacial impedance based on the compliant ionic adhesive. a) Schematic of the electrode and skin for sEMG and coupling process of the ionic fluxes in electrolytic tissue media and electronic current in the recording electrode. Due to the gaps at the interface, the induced charge-density greatly decreases when monitoring weak muscle activities. Consequently, the bioelectrical impedance ($Z_i=(1/R_{I\text{-}S}+sC_{I\text{-}S})^{-1}$, here $R_{I\text{-}S}$ is the resistance of interface, $C_{I\text{-}S}$ is the capacitance of the interface and s is the complex frequency of the stimulation waveforms) increases and induces the poor SNR sEMG signals. b) The graph shows the interfacial impedance and adhesion/thickness of different wet/dry electrodes. Green

circles represent the wet electrodes, red squares are the dry electrodes and the green star represents the Alg-PAAm compliant electrodes reported in this work. Blue area represents the impedance of human skin (5-10 kΩ), also it is the ideal impedance we want to reach. Clearly, for the dry electrode, the minimum impedance is ~25 kΩ at a thickness of 5 μm. However, the interfacial impedance cannot further decrease even the thickness reduces to 100 nm. Through increasing the adhesion between electrode and skin, we obtain a wet electrode with ultralow interfacial impedance (~20 kΩ).

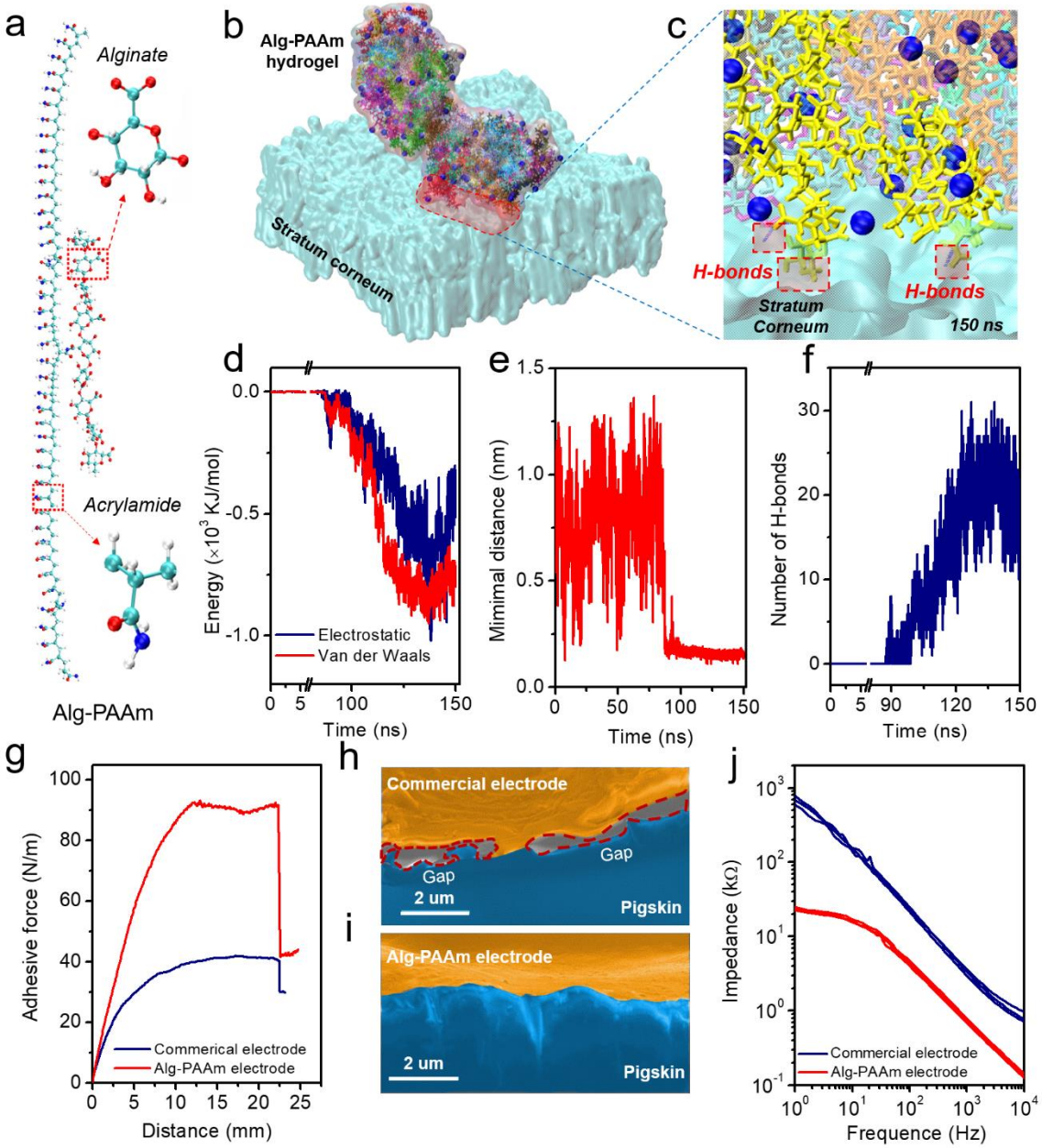

Figure 2. Simulated intermolecular interaction between Alg-PAAm hydrogel and stratum corneum. a) Simulation models for the alginate–polyacrylamide gel chain. b) Interaction between the Alg-PAAm adhesive hydrogel and SC at the molecular level. Initially, there were 25 alginate–polyacrylamide chains arranged with an average distance of 2 nm. Here we used different colors represented different chains. c) Detail of interaction between Alg-PAAm gel and SC at 150 ns, the highlight parts show the hydrogen bond (H-bonds). d) The Van der Waals (VDW) and electrostatic energy between the Alg-PAAm hydrogel and SC matrix. e) The minimal distance between the gel and the SC matrix. The minimal distance showed that the gel

well adhered to the SC matrix starting at the simulation time 90 ns. f) The number of hydrogen bonds (H-bonds) between the alginate–polyacrylamide gel and the SC matrix. g) 90° peel-off test of electrode based on Alg-PAAm gel and commercial gel shows the adhesion of Alg-PAAm is better than commercial h, i) SEM images show the interface between pigskin and commercial electrode (h) has many micron-scale gaps (red dotted lines) whereas it is no gaps for the interface with the Alg-PAAm compliant electrode (i). j) Graphs show the impedance of the electrode-skin system. Our Alg-PAAm electrode-skin system showed ~20 kΩ at 1 Hz while a poorly compliant commercial electrode-skin system showed ~500 kΩ at 1 Hz.

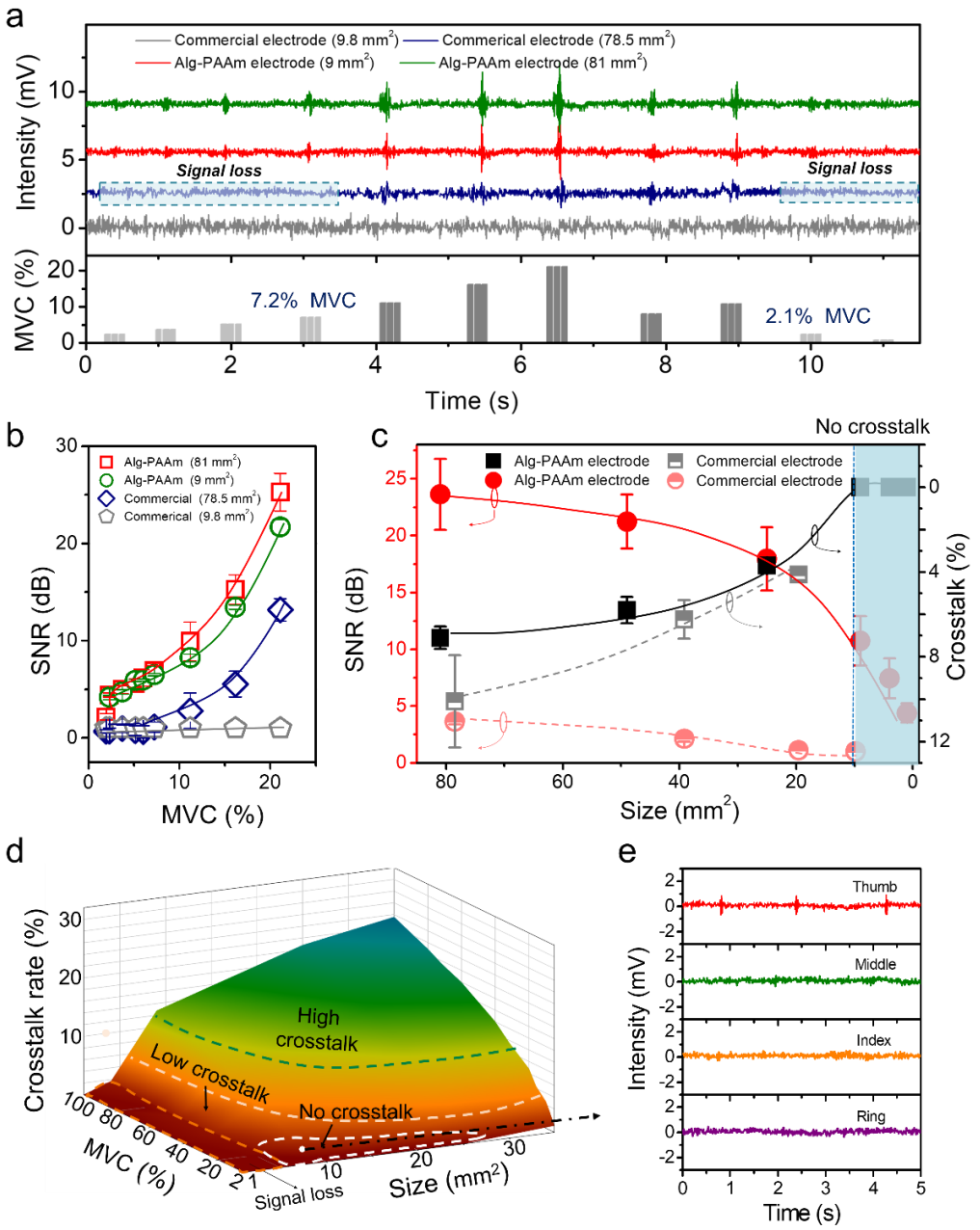

Figure 3. SNR and Crosstalk of the commercial electrode and different sized Alg-PAAm compliant electrode. a) Real-time sEMG recorded over time using different electrodes. The commercial electrode showed signal loss when the muscle contraction was below 7.2% MVC. The recording limit for the adhesive Alg-PAAm electrode was 2.1% MVC. b) SNR of sEMG signals collected using 81 mm^2 and 9 mm^2 Alg-PAAm electrodes, and 78.5 mm^2 and 9.8 mm^2 commercial electrodes at different muscle contractions. Alg-PAAm electrode had better SNR than the commercial electrode. c) The SNR and crosstalk of Alg-PAAm and commercial electrode with decreasing of size at 10% MVC. For both electrodes, the SNR will decrease but

crosstalk will weaken with decreasing of size. But the difference is that the Alg-PAAm electrode has SNR of ~3:1 even at 1 mm^2. For the commercial electrode, we cannot record any signals when the electrode size is smaller than 10 mm^2. Moreover, with the higher SNR, the Alg-PAAm compliant electrode can overcome the crosstalk after the size of the electrode smaller than 10 mm^2. d) Crosstalk rate of the middle finger caused by thumb finger with increasing the size of the electrode and the intensity of muscle contraction. The dull-red region is a signal loss region. The dark red region is a low crosstalk region highlighted by an orange dotted line. The dark red region ($4mm^2 \leq$ size ≤ 25 mm^2, 2% MVC $\leq$ muscle contraction $\leq$ 20% MVC) highlighted by a white dotted line is no crosstalk region. The region above the green dotted line is high crosstalk. e) The detail sEMG signals of thumb, index, middle and ring fingers at no crosstalk region. The electrode size is 9 mm^2 and muscle contraction at 10% MVC.

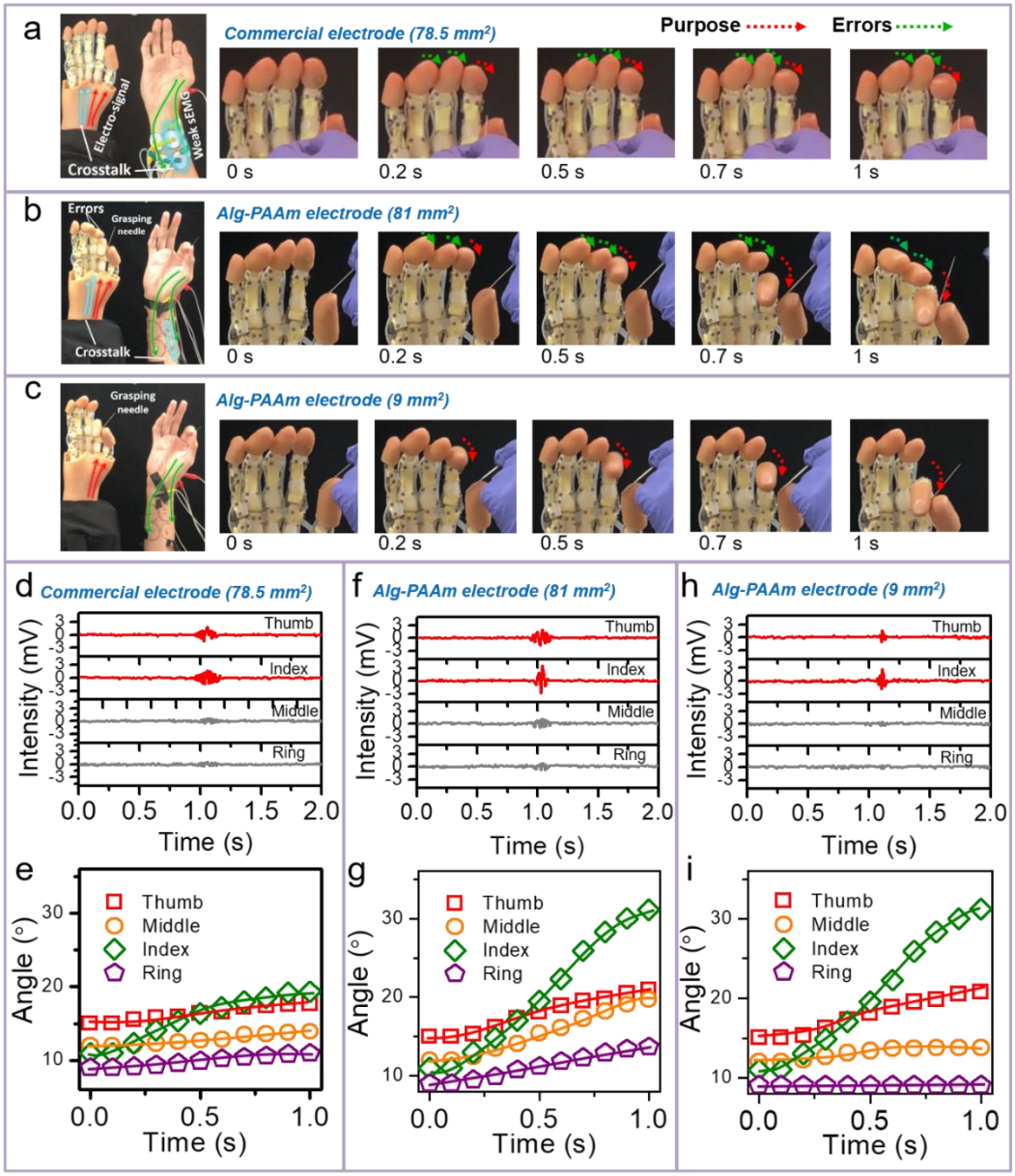

Figure 4. Driving the prosthetic hand to grasp a needle based on commercial and Alg-PAAm compliant electrodes and correlative sEMG signals. a) Needle grasping experiments based on commercial electrodes. Detail optical photograph of prosthetic fingers' movements. Although the prosthetic fingers moved along with the human fingers, due to poor compliance of commercial electrodes and their inability to record weak muscle activity, the prosthesis failed to grasp the needle. b) Needle grasping driven by sEMG signals obtained by 81 mm^2 Alg-PAAm electrodes. Due to high crosstalk, the middle and ring fingers in the prosthesis moved in error when the human hand grasped the needle. c) Needle grasping driven by sEMG signals obtained using 9 mm^2 Alg-PAAm electrodes. Small electrodes minimized crosstalk and

therefore, no errors were seen in the prosthetic fingers, allowing the prosthetic hand to successfully grasp the needle. d) sEMG data and e) bending angles obtained from four different fingers of the human hand while grasping a needle based on the commercial electrode. f) sEMG data and g) bending angles obtained from four different fingers of the human hand while grasping a needle based on 81mm^2 Alg-PAAm electrode. h) sEMG data and i) bending angles obtained from four different fingers of the human hand while grasping a needle based on the 9 mm^2 Alg-PAAm electrode.

The table of contents entry

A compliant ionic adhesive electrode, based on Alg-PAAm hydrogel, with ultralow interfacial impedance on the skin is created to record dynamically weak sEMG signals with high SNR and low crosstalk. Due to excellent properties, a prosthetic hand is successfully driven to inerrably grasp a needle based on the Alg-PAAm compliant electrodes.

Keyword: compliant electrode, bioelectronic impedance, surface electromyography, low noise, prosthetic control

L. Pan, P. Cai, L. Mei, Y. Cheng, Y. Zeng, M. Wang, T. Wang, Y. Jiang, B. Ji, D. Li,* and X. Chen*

A compliant ionic adhesive electrode with ultralow bioelectrode impedance

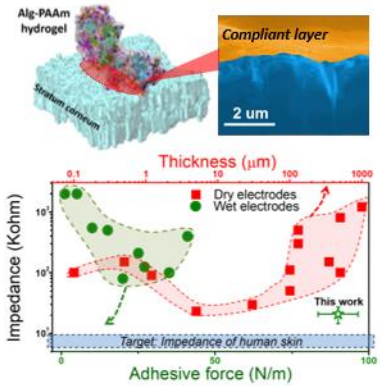

Supporting Information

A compliant ionic adhesive electrode with ultralow bioelectronic impedance

Liang Pan, Pingqiang Cai, Le Mei, Yuan Cheng, Yi Zeng, Ming Wang, Ting Wang, Ying Jiang, Baohua Ji, Dechang Li, and Xiaodong Chen**

Dr. L. Pan, Dr. P. Cai, Dr. Y. Zeng, Dr. M. Wang, Dr. T. Wang, Dr. Y. Jiang, Prof. X. Chen
Innovative Centre for Flexible Devices (iFLEX), Max Planck – NTU Joint Lab for Artificial Senses, School of Materials Science and Engineering, Nanyang Technological University, 50 Nanyang Avenue, 639798, Singapore
E-mail: chenxd@ntu.edu.sg

L. Mei
Biomechanics and Biomaterials Laboratory, Department of Applied Mechanics, Beijing Institute of Technology, Beijing 100081, China

Prof. B. Ji, Prof. D. Li
Institute of Applied Mechanics, Department of Engineering Mechanics, Zhejiang University, Hangzhou, 310027, China
E-mail: dcli@zju.edu.cn

Prof. B. Ji
Beijing Advanced Innovation Center for Biomedical Engineering, Beijing, 100191, China

Prof. Y. Cheng
Institute of High Performance Computing, A*STAR, 138632, Singapore

Supplementary Methods

Fabrication of Alg-PAAm electrode.

1) PDMS Substrate Fabrication: Illustration of the fabrication steps of the stretchable electrodes can be seen in Figure S7 PDMS (Poly-dimethyl Siloxane) is used as the buffer layer due to excellent stretchability. To create a PDMS substrate, mix liquid PDMS with the PMDS curing agent with a ratio of 10:1. The mixture is then stirred until it is homogeneous by using a centrifugal mixer. After the mixture is homogeneous, it is put inside the vacuum chamber to eliminate bubbles. It is then followed by the deposition of the PDMS layer on top of fluorinated silicon wafers. The fluorinated wafers are made by immersion of silicon wafer to a 10 mM solution of fluoroalkyl silane (heptadecafluoro-1,1,2,2-tetrahydro decyl trithoxysilane) in toluene for 30 minutes, followed by a heat treatment at 150˚C for 1 hour. The purpose of the fluorination is to create a hydrophobic surface. The deposition of PDMS is done by spin coating at 1000 rpm on top of fluorinated wafers for 40 seconds. The final step is to let it cure at 60 ˚C for 4 hours.

2) Deposition of Au/Cr, Insulator: Deposition of the gold layer on top of PDMS substrate is done by using the sputtering technique. A very thin layer (in the scale of nm) is needed to preserve its compliance; ability to conduct even when it is stretched. Before the gold layer is sputtered, a 5 nm Chromium layer is deposited on top of PDMS to increase the adhesion between PDMS and the gold layer for better contact. Finally, the gold layer with a thickness of 200 nm is sputtered by using a sputtering machine. A mask (Figure S7) is used in the sputtering process to control and pattern the deposition of gold in the desired area. Next, on top of the gold layer, an insulating layer (HfO_2) is deposited as an insulating layer to prevent the gold that is connected to the device from collecting any signal from the surface of the skin.

3) Deposition of Alg-PAAm hydrogel: After the first component of the electrode (metal) is deposited, the next step is to deposit the highly adhesive Alg-PAAm hydrogel. Before the

hydrogel is deposited, the PDMS is treated with 10 wt% benzophenone in ethanol solution. The purpose of benzophenone is to address the oxygen inhibition problem that is often found in elastomers and also to acts as an ultraviolet assisted grafting agent for chemical crosslinking of the hydrogel on elastomers surfaces.[1] When the benzophenone is exposed to UV irradiation, it is excited into a singlet state which is later converted into a triplet state through the intersystem crossing. Through hydrogen abstraction from surrounding C-H bonds in the elastomer, it changes form from triplet state into benzophenone ketyl radical. Then the radical initiate the grafting process of the polymer networks in hydrogel onto the reactive surface of the elastomer, generating benzopinacol.[1]

Fabrication of Alginate PAAm (Ca-based) hydrogels was done in one step, by mixing water with sodium alginate, ionic cross-linker, covalent cross-linker, acrylamide, thermos-initiator, and 10%wt LiCl to further increase the ionic conductivity of the hydrogel. The addition of ionic and covalent cross-linker is to cross-link alginate and PAAm network respectively. Alginate chains will be ionically crosslinked by Ca^{2+} will interpenetrate with covalently crosslinked PAAm network. The result is Ca-alginate PAAm that has exceptional toughness.

After the fabrication of the Ca-Alg PAAm hydrogel, both the hydrogel and PDMS along with the metal is assembled, followed by UV irradiation to crosslink the polymer network in the hydrogel and to increase the adhesion to the surface of the PDMS which will lead to a robust interface capable of large deformation.

Characterization of cross-section morphology and adhesive force of the Alg-PAAm electrode.

We used the Field Emission Scanning Electron Microscope (SEM) to characterize the cross-section of the Alg-PAAm electrode / commercial electrode and bionic skin. SEM images shown in Figure 2h and 2i were obtained on a Zeiss SUPRA55 SEM using an acceleration

voltage of 5 kV. More detailly, we use a sharp blade to cut the sample for SEM under liquid nitrogen.

The adhesive force of different electrode and bionic skin (Figure 2g, Figure S5 and Figure S6) were obtained using an Instron mechanical tester (MTS criterion Model 42) with 50 N load cell and 100 N Bionix vice grips.

Molecular dynamics (MD) Simulation models and methods

The all-atom model for the alginate–polyacrylamide hydrogel is built up by self-assemble of the alginate–polyacrylamide chains. Each single alginate–polyacrylamide chain is built up by 9 alginate monomers and 45 acrylamide monomers (see Figure 2a), which yield the ratio of acrylamide/(acrylamide + alginate) (wt%) equal to about 65%, according to the previous study[2]. The poly-alginate and polyacrylamide chains are cross-linked in the middle by covalent bonds, as shown in Figure 2a. The alginate–polyacrylamide hydrogel structure formed through self-assembly of the alginate–polyacrylamide chains, as shown in Figure S2a. Figure S2b to S2d illustrates the atomistic of the alginate–polyacrylamide hydrogel structure. To model the skin's surface layer, i.e., the Stratum Corneum (SC), we built up the lipid matrix of SC according to previous studies. In this study, the lipid matrix of SC is mixed by cholesterol (CHOL), free fatty acid (FFA), and ceramides (CER) at a 1:1:1 ratio, which is built up by the CHARMM-GUI web service.[3] The size of the lipid matrix of SC is about 15×15 nm^2.

The MD simulations were performed by the GROMACS package, [4,5] with the force field CHARMM36m [6] for the lipid layer and the Consistent Valence force field (CVFF) [7] for the alginate–polyacrylamide hydrogel. TIP3P water molecules [8] were used to solvate the simulated structure, and the appropriate number of calcium ions (Ca^{2+}) was added to neutralize the system. All the simulations were performed in periodic boundary conditions with the NPT ensemble. The pressure was coupled in 1 bar by the Parrinello-Rahman method, [9] and the temperature was coupled in 300K by the V-rescale algorithm.[10] The LINCS algorithm is used to restrain the covalent bonds of hydrogen atoms.[11] The time step is set to 2 fs. The cutoff of

the non-bonded interactions is set to 1.2 nm. The particle mesh Ewald (PME) method [12] was applied to calculate the long-range electrostatic interaction. The graphics and visualization analysis were performed by the Visual Molecular Dynamics (VMD) package.[13]

Supplementary Figures

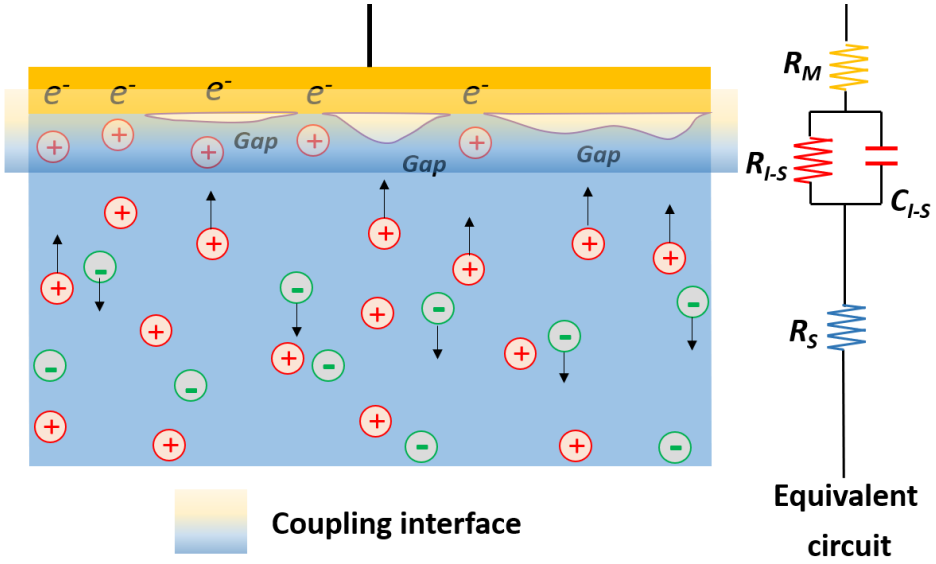

Figure S1. Graph shows the coupling process of the ionic fluxes in electrolytic tissue media of our body and electronic current in recording dry electrode. The difference is that there is no ionic conducting layer between electrode and skin. The right panel shows the equivalent circuit.

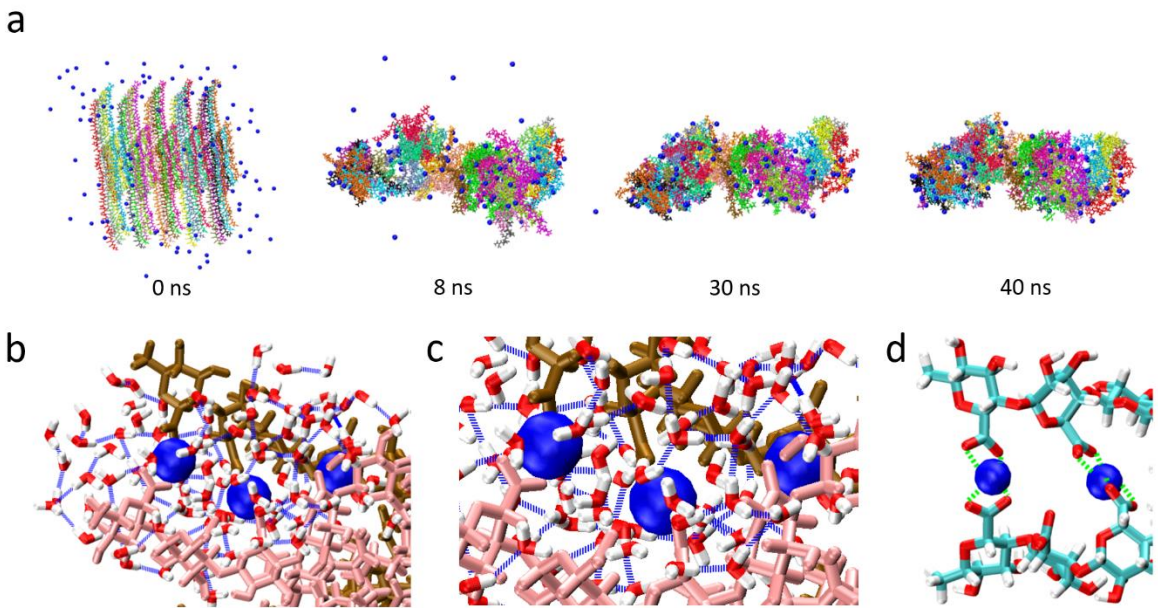

Figure S2. Molecular structure of alginate-polyacrylamide. a) The process of the self-assemble of the alginate–polyacrylamide chains. Initially, there were 25 alginate–polyacrylamide chains arranged with an average distance of 2 nm. Each chain was represented by individual color. The blue dots represented the Ca^{2+} ions. b) and c) The zoom-in view of the atomistic structure of the alginate–polyacrylamide gel by MD simulations. The blue dash lines represented the hydrogen bond network by water molecules. d) The detailed structure of two alginate–polyacrylamide chains cross-linked by Ca^{2+} ions. The polar interactions that bridged the two chains were represented by green dash lines.

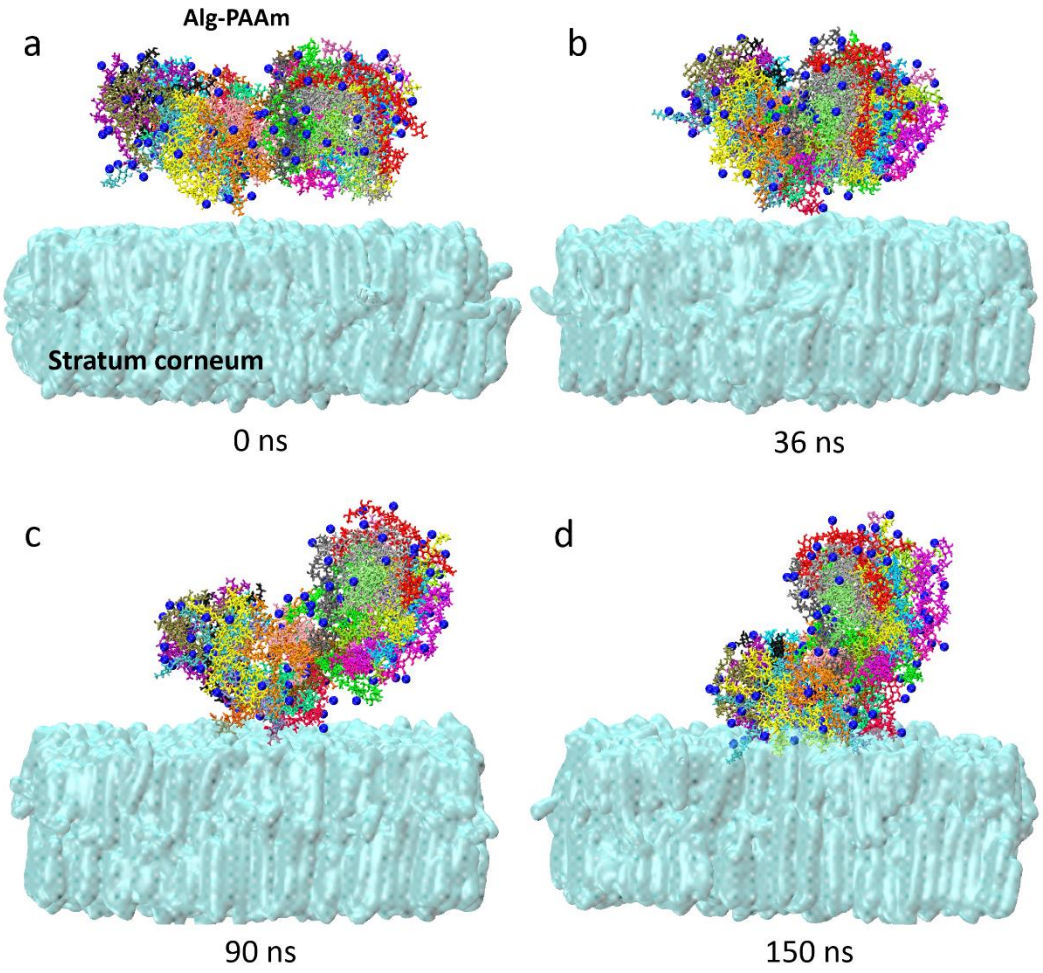

Figure S3. Process of the alginate–polyacrylamide gel adheres to the SC matrix at 0 ns (a), 36 ns (b), 90 ns (c) and 150 ns (d).

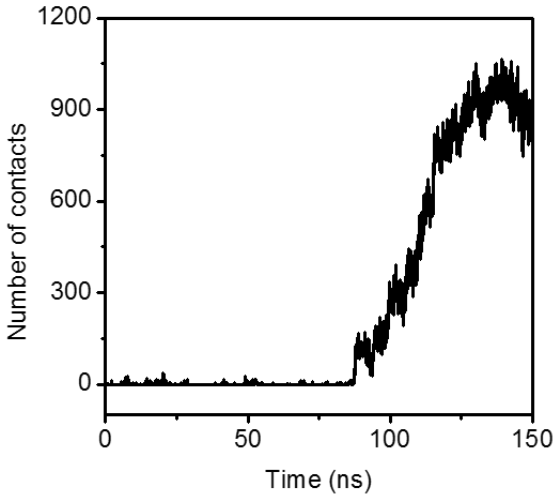

Figure S4. The number of atom contacts between the alginate–polyacrylamide gel and the SC matrix.

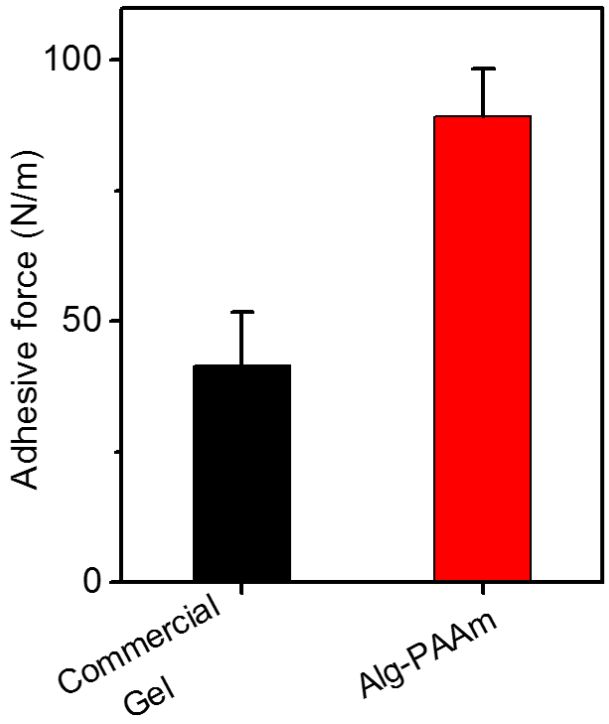

Figure S5. 90° peel-off test of electrode based on Alg-PAAm hydrogel and commercial gel shows adhesion of Alg-PAAm is better than commercial gel based on more than 10 samples.

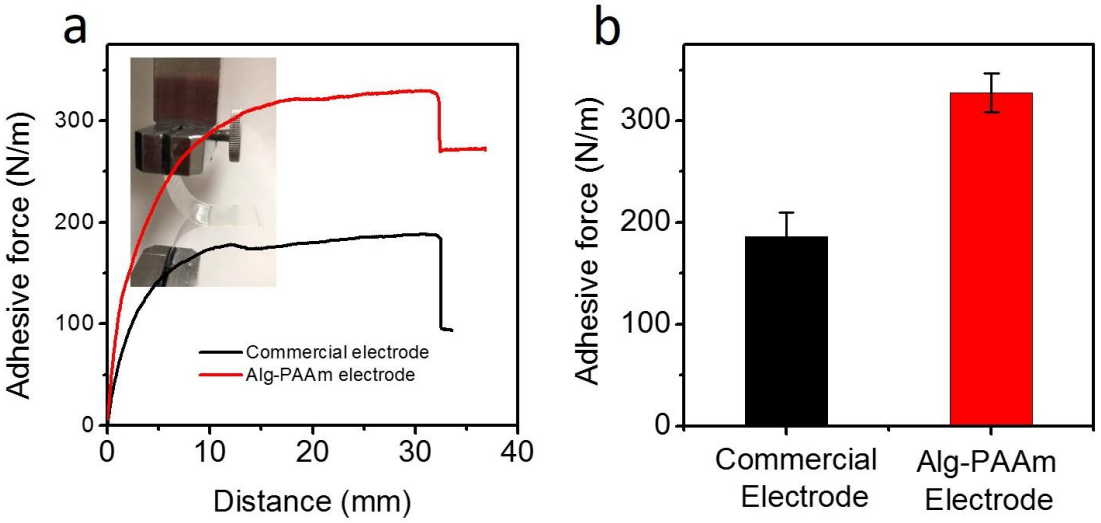

Figure S6. 180° peel-off test of electrode based on Alg-PAAm and commercial electrodes. Clearly, the commercial electrode shows poorer adhesive force than the Alg-PAAm electrode. This result agreed well with that of a 90° peel-off test shown in Figure 2g and Figure S5.

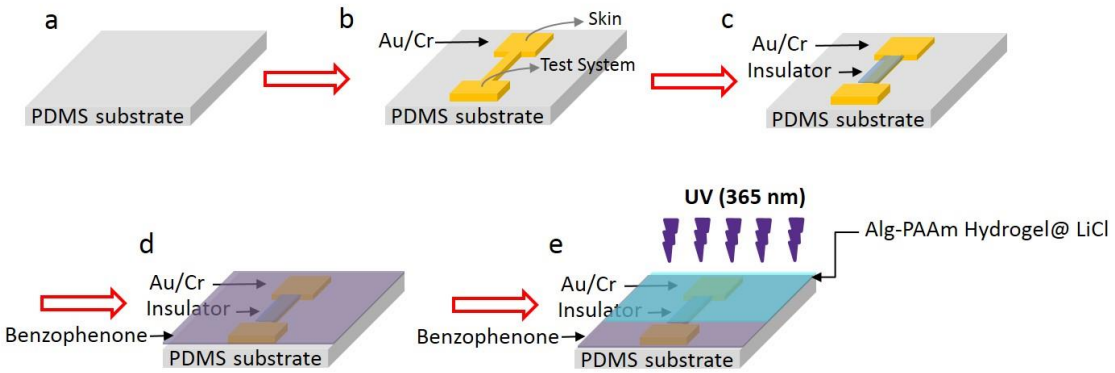

Figure S7. Fabrication of Alg-PAAm electrode. a) 20 μm PDMS was used as the buffer layer due to excellent stretchability. To create a PDMS substrate, mix liquid PDMS with the PDMSS curing agent with a ratio of 10:1. b) 200 nm/5nm Au/Cr pattern was deposited on to PDMS. Cr layer was deposited on top of PDMS to increase the adhesion between PDMS and the gold layer for better contact. The top of the pattern was contacted with the skin for recording sEMG, the bottom of the pattern was connected to the test system. c) An insulating layer (HfO_2) was deposited on the gold layer to overcome the unnecessary contact between the other part of the gold pattern and skin. d) PDMS is treated with 10 wt% benzophenone in ethanol solution. The purpose of benzophenone is to address the oxygen inhibition problem that is often found in elastomers and also to acts as an ultraviolet assisted grafting agent for chemical crosslinking of the hydrogel on elastomers surfaces. e) Followed by UV irradiation to crosslink the polymer network in the hydrogel and to increase the adhesion to the surface of the PDMS which will lead to a robust interface capable of large deformation.

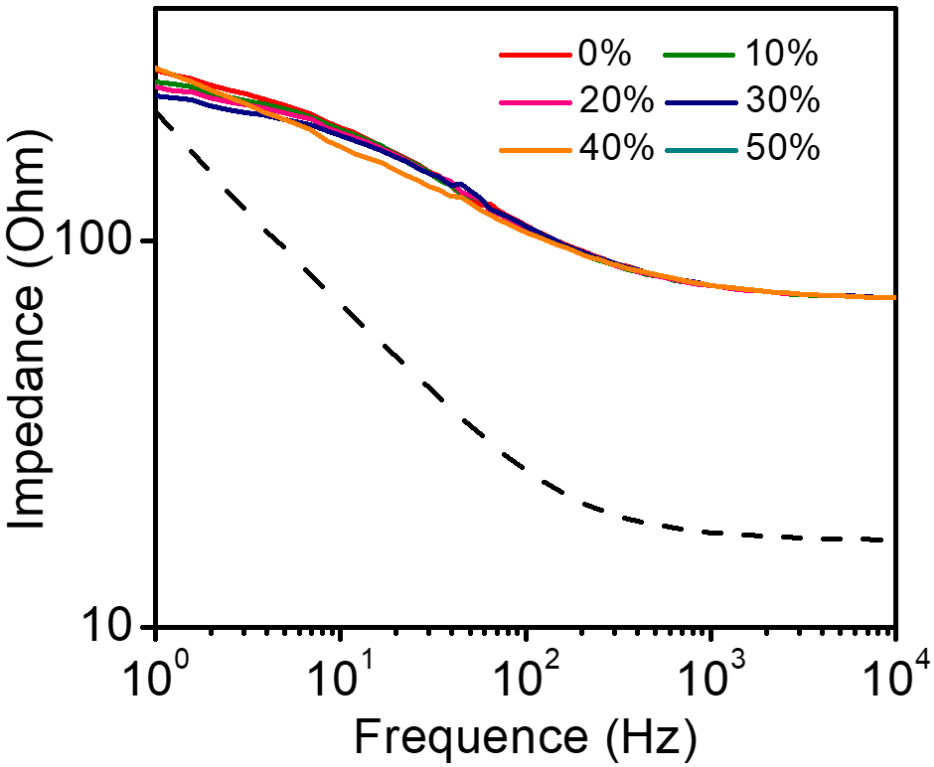

Figure S8. The impedance of commercial electrode (the dash curve) and Alg-PAAm compliant electrode. Intrinsic impedance of commercial electrode and Alg-PAAm electrode under different strain. Because of the rigidity of a commercial electrode, we measured the impedance of it with no strain. For the Alg-PAAm electrode, the impedance was nearly unchanged with strain from 0 to 50% which was enough for the movement of the human body. And the intrinsic impedance of the tow type electrode was about 10~200 Ohm from 1 Hz to 10^4 Hz which was too low to affect the recording of the sEMG signals.

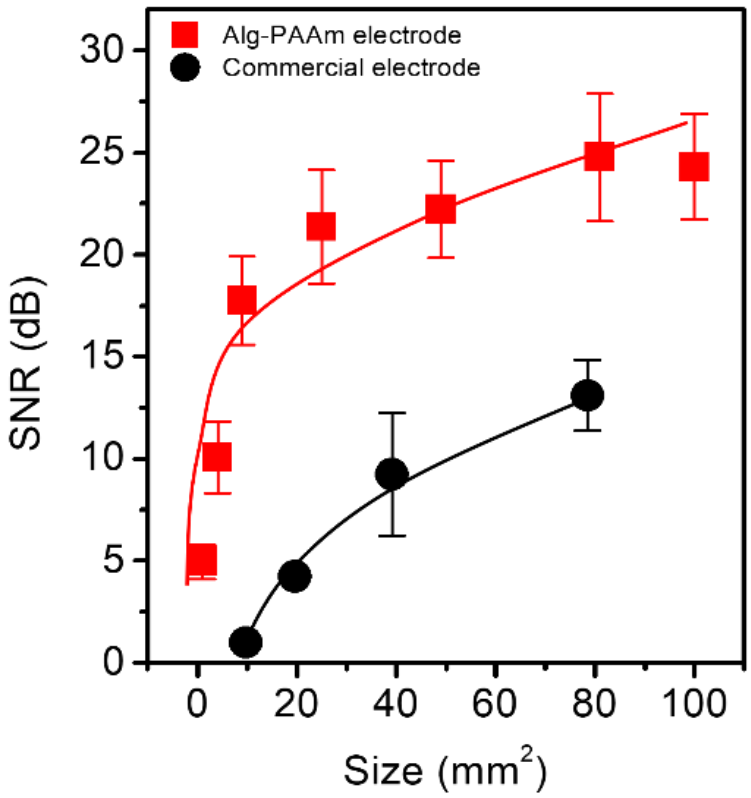

Figure S9. SNR as a function of electrode area for commercial and Alg-PAAm electrode at 20% MVC. SNR improved with a larger electrode area. Alg-PAAm electrodes ≥9 mm^2 showed better SNR than commercial electrodes that were 78.5 mm^2 large.

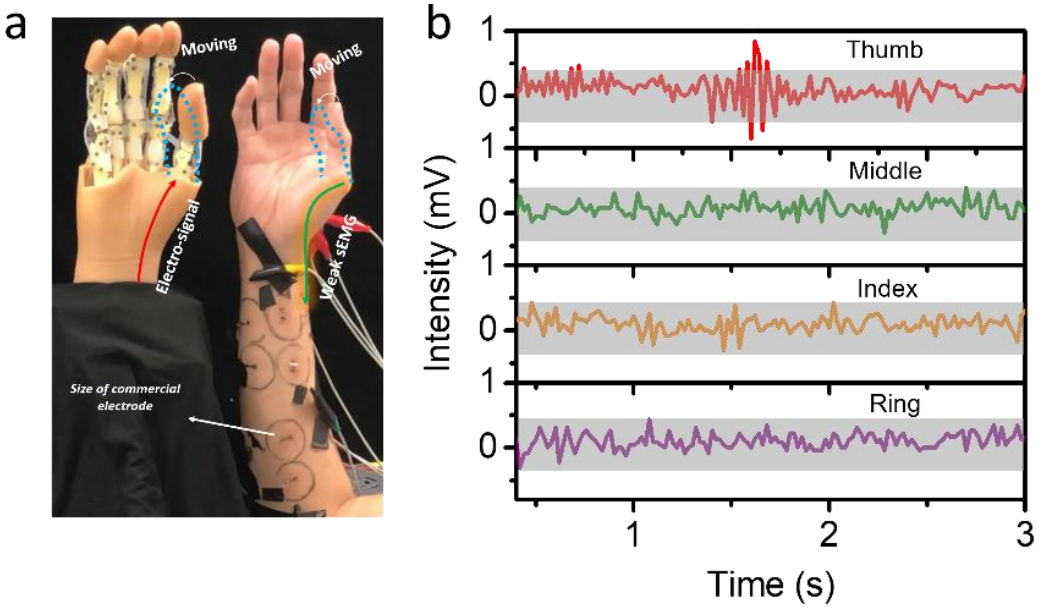

Figure S10. Driving the movement of a prosthetic hand by Alg-PAAm electrode. a) Photograph of a human hand (right) driving the movement of a prosthetic hand at 5% MCV. The green arrow indicates the weak sEMG signal from the thumb. The red arrow represents driving electrical signals from the control system. Black circles are traces showing the size of commercial electrodes. Blue dotted lines indicate the movement of the fingers. b) sEMG signals recorded from different fingers of the human hand using the Alg-PAAm electrode that is 81 mm^2 large. The tests on human skin were approved by Institute of Review Board, Nanyang Technological University (approval number: IRB-2017-08-035-01).

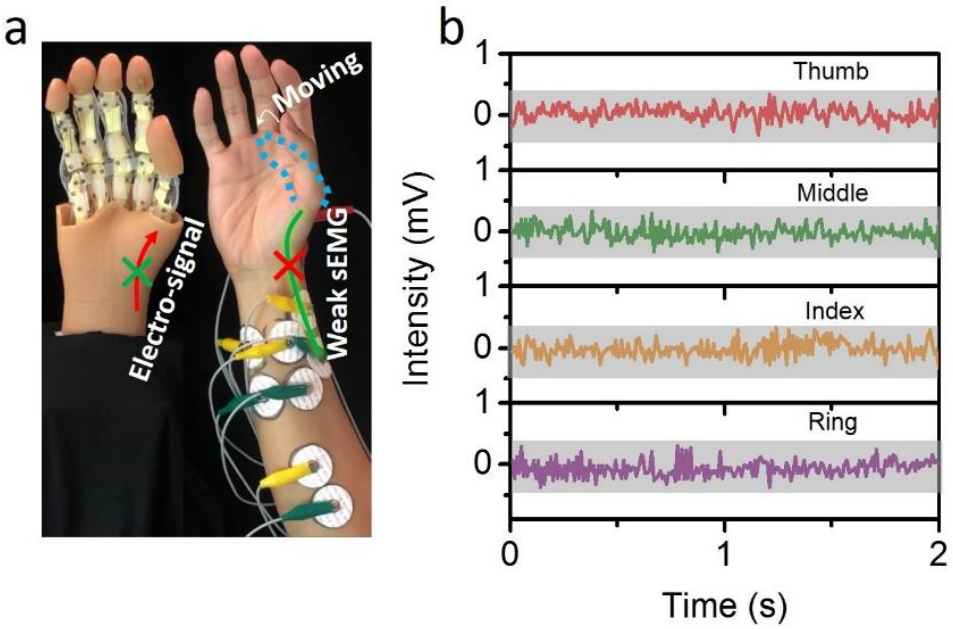

Figure S11. Driving the movement of a prosthetic hand by the commercial electrode. a) Photograph of a human hand (right) driving the movement of a prosthetic hand at 5% MCV. Due to the high interfacial impedance of commercial electrodes, no sEMG signals were recorded and therefore, the prosthesis could not be driven to perform any activities alongside the human hand**.** b) sEMG signals recorded from different fingers of the human hand using the commercial electrode with 78.5 mm^2.

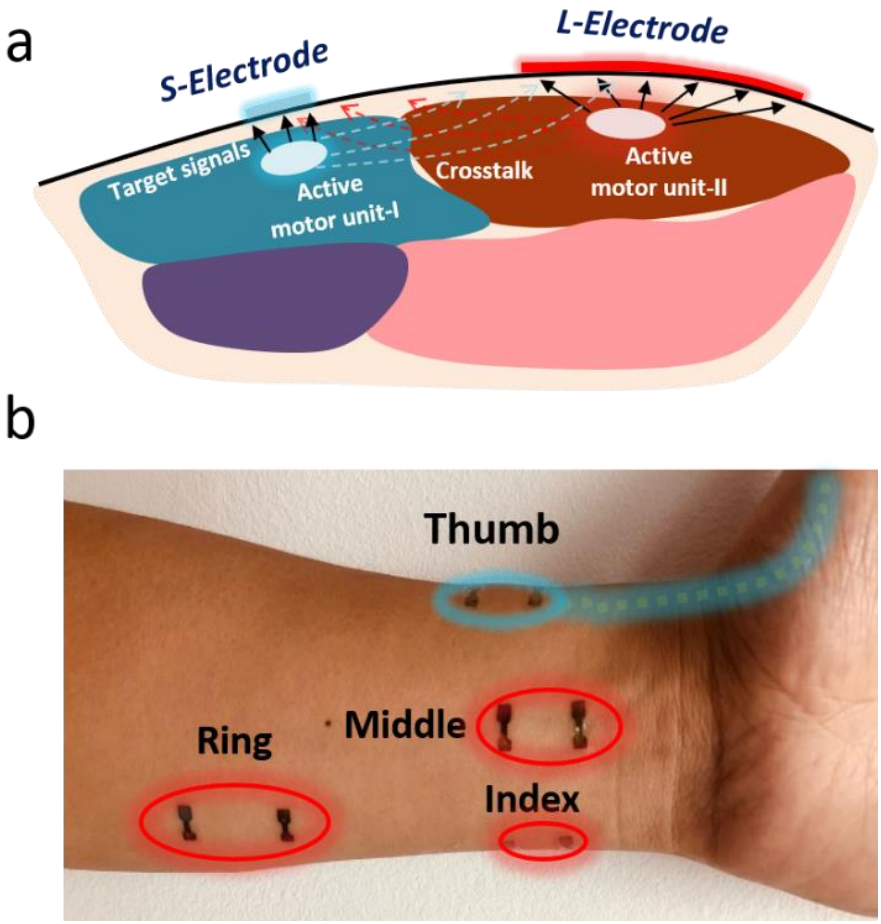

Figure S12. a) Schematic of crosstalk between two electrodes. S-electrode means a small-sized electrode, L-electrode means a large-sized electrode. Compared to S-electrode, L-electrode can record more signals. However, L-electrode has more serious crosstalk. b) Photograph showing how crosstalk is measured. As the thumb is moved at various strengths (blue, abductor pollicis longus), sEMG signals were recorded from the Middle, Index and Ring fingers to assess the intensity of the crosstalk between the muscles of these fingers.

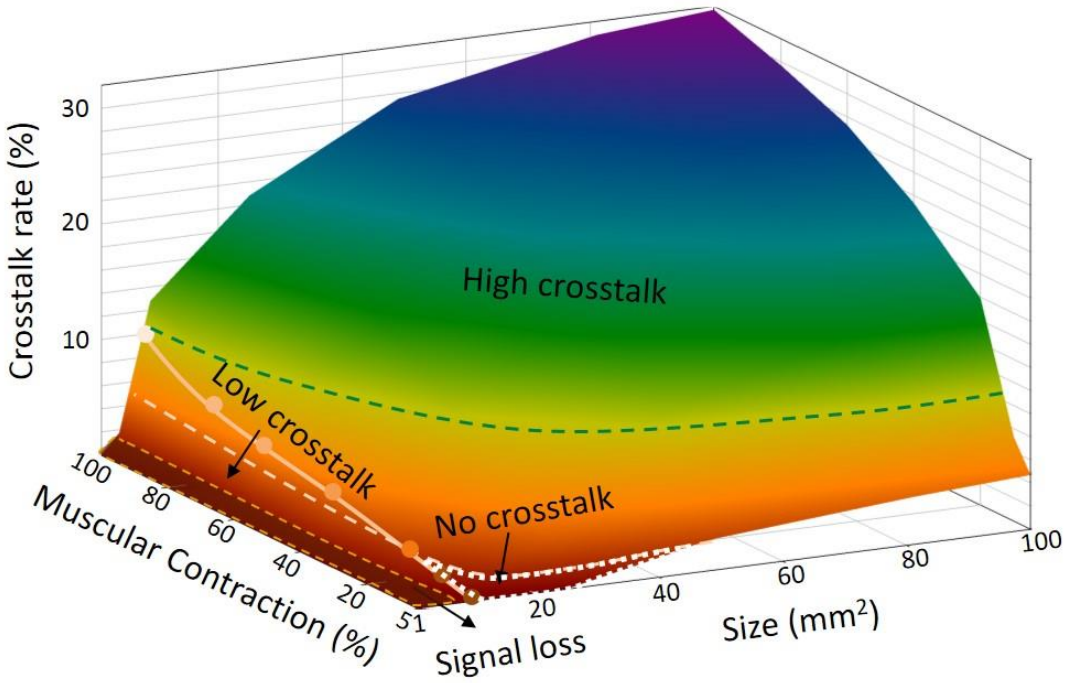

Figure S13. Crosstalk rate of the middle finger caused by thumb finger with increasing the size of the electrode and the intensity of muscle contraction. The dull-red region is a signal loss region. The dark red region is a low crosstalk region highlighted by an orange dotted line. The dark red region ($4mm^2 \leq$ size ≤ 25 mm^2, 2% MVC $\leq$ muscle contraction $\leq$ 20% MVC) highlighted by a white dotted line is no crosstalk region. The region above the green dotted line is high crosstalk.

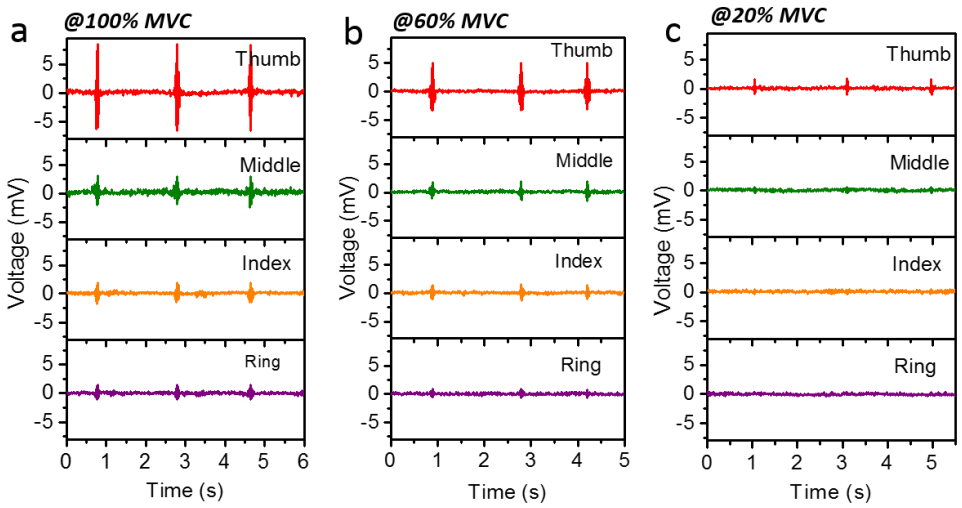

Figure S14. The detail sEMG signals of thumb, middle, index and ring fingers at 100% MVC (a), 60% MVC (b) and 20%MVC (c) based on 9 mm^2 Alg-PAAm electrodes.

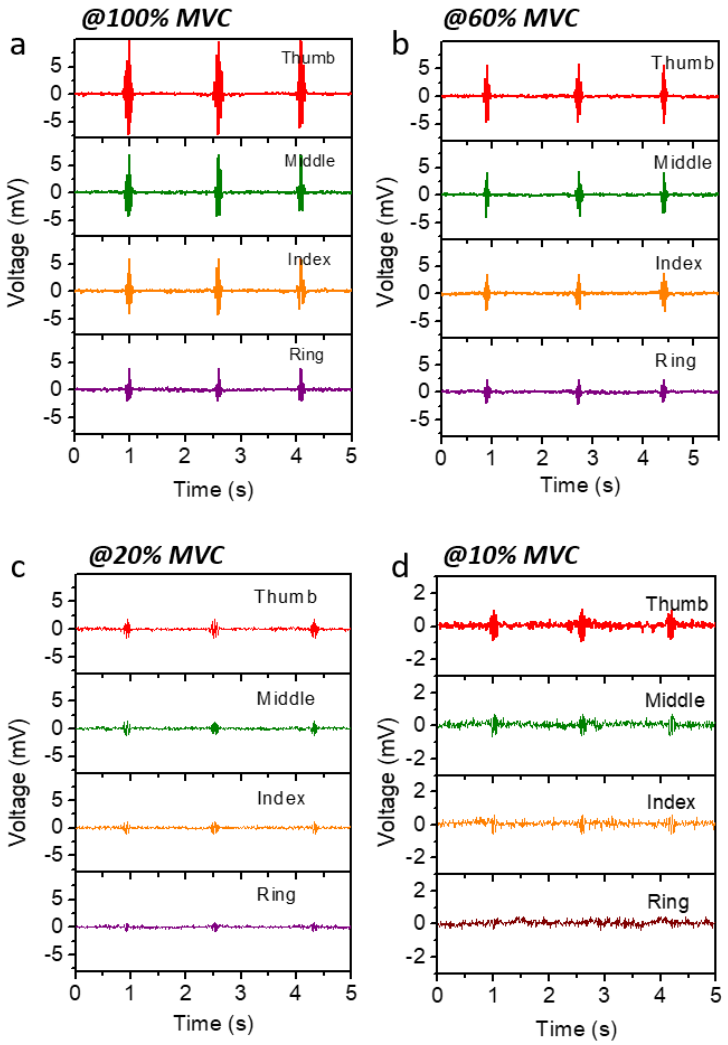

Figure S15. The detail sEMG signals of thumb, middle, index and ring fingers at 100% MVC (a), 60% MVC (b), 20%MVC (c) and 10%MVC based on 81 mm^2 Alg-PAAm electrodes. As compared to Figure 3d, the scale of the x-axis in (d) is also from -3 mv to 3 mv.

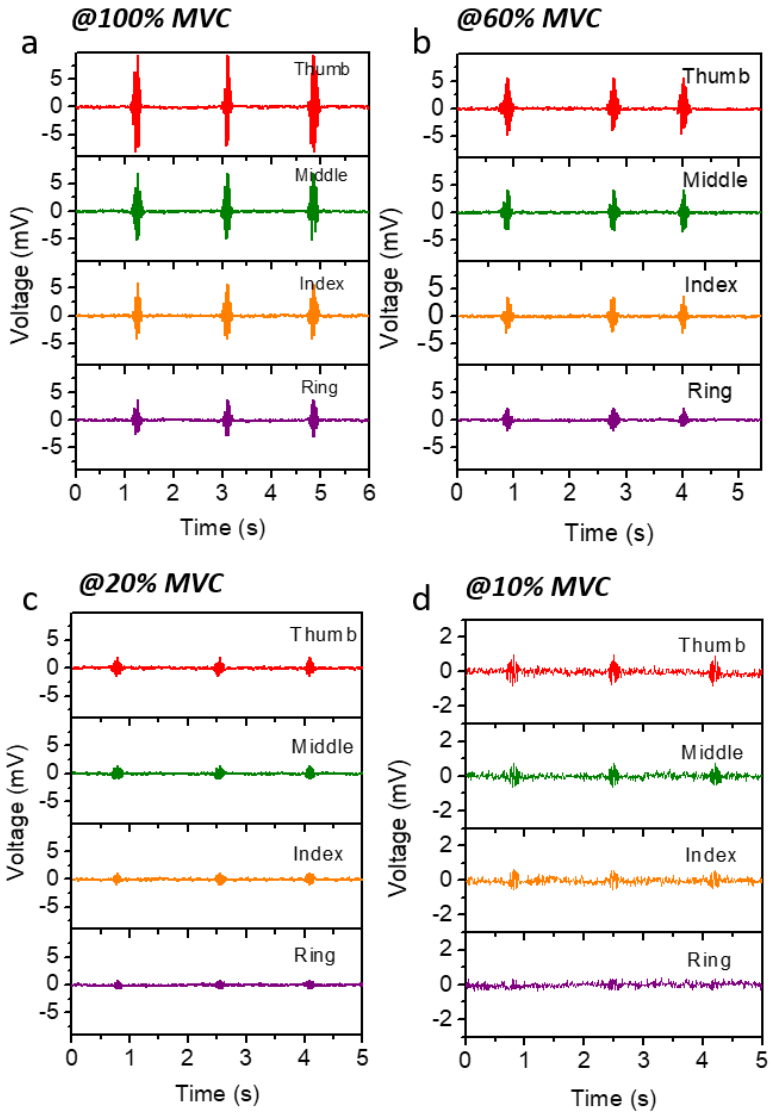

Figure S16. The detail sEMG signals of thumb, middle, index and ring fingers at 100% MVC (a), 60% MVC (b), 20%MVC (c) and 10%MVC based on 78.5 mm^2 Alg-PAAm electrodes. As compared to Figure 3d, the scale of the x-axis in (d) is also from -3 mv to 3 mv.

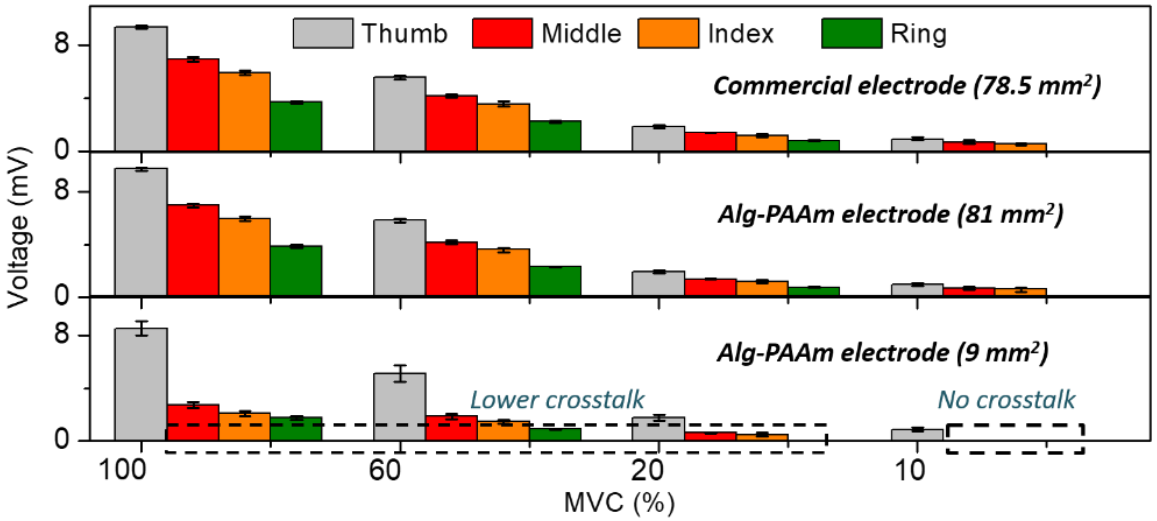

Figure S17. Statistical data of crosstalk measured using different sized commercial and Alg-PAAm electrodes. The smaller 9 mm^2 Alg-PAAm electrode showed lower crosstalk than the larger 81 mm^2 Alg-PAAm electrode and 78.5 mm^2 commercial electrode. Crosstalk disappeared at muscle contraction below 10%.

Table S1. The difference of wet electrode and dry electrode

	Wet electrode	Dry electrode
ionic conducting layer	Yes	No
Monitoring	Dynamic state	Static state
Cost	Low, ~0.5 SGD	High, 20~100 SGD
Cycles	<10 times	>100 times
Durability	Low, 1~4 h	High, >24h
Convenience	No, needing clean the skin after using	Yes, no disposition
Application	Clinical, for diagnose, prosthetic controlling and so on.	Consumer electronics, for I/O control.

Table S2. The electrode-skin impedance and thickness of the dry electrode

	Electrode	Thickness (μm)	Impedance* (KOhm)	Reference
1	AgNW/PDMS	1,000	1,000	C. Myers, H. Huang, Y. Zhu, *RSC Adv.* **2015**, *5*, 11627.
2	PEDOT:PSS/Textile	500	800	E. Bihar *et al.* Flex. Print. Electron. 2018, *3*, 034004.
3	Graphene	130	500	D. Kuzum *et al. Nat. Commun.* 2014, *5*, 1.
4	Doped-Graphene	130	300	D. Kuzum *et al. Nat. Commun.* 2014, *5*, 1.
5	Graphene/Textile	300-400	140	M. K. Yapici, T. Alkhidir, Y. A. Samad, K. Liao, *Sens. Actuators B Chem.* 2015, *221*, 1469.
6	Carbon/ppEDOT	100	110	L. Bareket *et al. Sci. Rep.* 2016, *6*, 25727.
7	EES	500	100	J. W. Jeong *et al. Adv. Mater.* 2013, *25*, 6839
8	EES	100	50	J. W. Jeong *et al. Adv. Mater.* 2013, *25*, 6839
9	EES	30	27	J. W. Jeong *et al. Adv. Mater.* 2013, *25*, 6839
10	EES	5	24	J. W. Jeong *et al. Adv. Mater.* 2013, *25*, 6839
11	Fe@Sibione	1.2	200	K. I. Jang et al. Adv. Funct. Mater. 2016, 26, 7281
12	GET	0.5	150	S. Kabiri Ameri *et al. ACS nano* 2017, *11*, 7634.
13	PVA-Au nanomesh	0.1	100	A. Miyamoto *et al. Nat. Nanotech.* 2017, *12*, 907.
14	Alg-PAAm electrode	~	~20	This work

*The impedance is estimated value from the data of current typical dry electrode provided in the reference.

Table S3. The electrode-skin impedance and adhesion of the wet electrode

	Electrode	Adhesive force* (N/m)	Impedance** (KOhm)	Reference
1	CNT/aPDMS	1.1	2,000	S. M. Lee *et al. Sci. Rep.* **2014**, *4*, 6074
2	PDMS_40NW	5	2,000	J.-H. Kim *et al. Nano Lett.* **2018**, *18*, 4531.
3	PDMS_40NW/Tape	15	500	J.-H. Kim *et al. Nano Lett.* **2018**, *18*, 4531.
4	Au/Parylene	10	550	R. A. Nawrocki *et al*. *Adv. Funct. Mater.* **2018**, *28*, 1803279.
5	NEE	20	100	L. Liu *et al. Small*, **2019**, *15*, 1900755.
6	Silk/Au	25	210	G. Chen *et al. Adv. Mater.* **2018**, *30*, 1800129.
7	PDA-rGO-PAM	27	125	L. Han *et al. Small* **2017**, *13*, 1601916.
8	a4-PDMS_40NW	35	100	J.-H. Kim *et al. Nano Lett.* **2018**, *18*, 4531.
9	Commercial electrode	41	500	As a controlled experiment in this work
10	Alg-PAAm electrode	~90	~20	This work

*The adhesive force is estimated value from the data given by the previous works

** The impedance is estimated value from the data of the current typical wet electrode provided in the reference.

Supplementary References

[1] H. Yuk, T. Zhang, G. A. Parada, X. Liu, X. Zhao, *Nat. Commun.* **2016**, *7*, 1.
[2] J. Y. Sun, X. H. Zhao, W. R. K. Illeperuma, O. Chaudhuri, K. H. Oh, D. J. Mooney, J. J. Vlassak, Z. G. Suo, *Nature* **2012**, *489*, 133.
[3] S. Jo, T. Kim, V. G. Iyer, W. Im, *J. Comput. Chem.* **2008**, *29*, 1859.
[4] S. Pronk, S. Pall, R. Schulz, P. Larsson, P. Bjelkmar, R. Apostolov, M. R. Shirts, J. C. Smith, P. M. Kasson, D. van der Spoel, B. Hess, E. Lindahl, *Bioinformatics* **2013**, *29*, 845.
[5] M. J. Abraham, T. Murtola, R. Schulz, S. Páll, J. C. Smith, B. Hess, E. Lindahl, *SoftwareX* **2015**, *1-2*, 19.
[6] J. Huang, S. Rauscher, G. Nawrocki, T. Ran, M. Feig, B. L. de Groot, H. Grubmuller, A. D. MacKerell, *Nat. Methods* **2017**, *14*, 71.
[7] A. T. Hagler, S. Lifson, P. Dauber, *J. Am. Chem. Soc.* **1979**, *101*, 5122.
[8] W. L. Jorgensen, J. Chandrasekhar, J. D. Madura, R. W. Impey, M. L. Klein, *J. Chem. Phys.* **1983**, *79*, 926.
[9] M. Parrinello, A. Rahman, *J. Appl. Phys.* **1981**, *52*, 7182.
[10] G. Bussi, D. Donadio, M. Parrinello, *J. Chem. Phys.* **2007**, *126*.
[11] B. Hess, *J.Chem. Theory Comput.* **2008**, *4*, 116.
[12] U. Essmann, L. Perera, M. L. Berkowitz, T. Darden, H. Lee, L. G. Pedersen, *J. Chem. Phys.* **1995**, *103*, 8577.
[13] W. Humphrey, A. Dalke, K. Schulten, *J. Mol. Graph. Model.* **1996**, *14*, 33.